- 1 Solar-induced chlorophyll fluorescence detects photosynthesis variations and
- 2 drought effects in tropical rubber plantation and natural deciduous forests
- 3 Xueqian Wang^{1,*}, Peter D. Blanken¹, Jeffrey D. Wood², Yann Nouvellon^{3,4,5}, Philippe Thaler^{3,4,5},
- 4 Frédéric Gay^{3,4,5}, Poonpipope Kasemsap⁶, Amnat Chidthaisong^{7,8}, Pakorn Petchprayoon⁹,
- 5 Chompunut Chayawat⁹, Jingfeng Xiao¹⁰, Xing Li¹¹
- 6 Department of Geography, University of Colorado, Boulder CO 80309, USA
- ²School of Natural Resources, University of Missouri, Columbia, MO, USA.
- 8 ³ Eco&Sols, Univ Montpellier, CIRAD, INRAE, IRD, Institut Agro, F-34060 Montpellier, France
- 9 ⁴ CIRAD, UMR Eco&Sols, F-34060 Montpellier, France
- ⁵ Hevea Research Platform in Partnership, Kasetsart University, Bangkok 10900, Thailand
- 11 ⁶ Department of Horticulture, Faculty of Agriculture, Kasetsart University, Bangkok 10900,
- 12 Thailand
- 13 ⁷ The Joint Graduate School of Energy and Environment, King Mongkut's University of
- 14 Technology Thonburi (KMUTT), Bangkok 10140, Thailand
- 15 8 Center for Climate Change Technology and Innovation, King Mongkut's University of
- 16 Technology Thonburi (KMUTT), Bangkok 10140, Thailand
- 17 ⁹Geo-Informatics and Space Technology Development Agency, Bangkok 10210, Thailand
- 18 ¹⁰ Earth Systems Research Center, Institute for the Study of Earth, Oceans, and Space, University
- 19 of New Hampshire, Durham, NH 03824, USA
- 20 ¹¹Research Institute of Agriculture and Life Sciences, Seoul National University, Seoul, South
- 21 Korea

22

23 Corresponding author: Xueqian Wang (E-mail address: xueqian.wang@colorado.edu)

24

- 25 **Abstracts:** Past assessments of the global carbon balance have shown to have high uncertainty
- 26 particularly in the Mainland Southeast Asia (MSEA) owing to the increasing climate extremes and
- 27 land use changes. Recently, remotely sensed solar-induced chlorophyll fluorescence (SIF) and
- 28 near-infrared reflectance of vegetation (NIR_v) have been found to have great potential to assess
- 29 the dynamics of vegetation gross primary production (GPP). Using flux tower GPP from two
- 30 rubber plantation and one natural forest sites, our study assessed the utility of SIF and NIR_v to

detect GPP and drought stress for these two major land uses in this tropical monsoon region, and the underlying mechanistic link among SIF, NIR_v, and GPP based on path analysis. The results indicate that the native SIF from OCO-2 satellite and its two derived finer-resolution SIF products (i.e., GOSIF and $\overline{SIF}_{oco2\ 005}$) outperformed the normalized difference vegetation index (NDVI) and the enhanced vegetation index (EVI) in detecting GPP and drought effects at the rubber plantation sites. Although the young natural forest exhibited much lower EVI and NIR_v, it had comparable magnitude of GPP to the rubber plantations, which was captured by SIF. Path analysis shows that the SIF-GPP relationship was mainly controlled by NIR_v, which represents the canopy structural effects including both the absorption and scattering traits. In line with site-scale analysis, the regional patterns indicated higher consistency between SIF and NIR_v than EVI for the tropical forests. The quantum yield of SIF (\emptyset_F) was sensitive to precipitation anomaly, while its negative effect on photosynthesis was offset by high PAR under drought. Both tropical deciduous forest and plantation forest were more vulnerable to drought than evergreen forest. We highlight the usage of NIR_v and SIF for monitoring canopy structure and photosynthesis, respectively, and the needs of higher-resolution observations to reduce the uncertainties in quantifying SIF-GPP relationships.

Keywords: Tropical deciduous forest, Plantation forest, Sun-induced fluorescence, Gross primary production, Drought

1 Introduction

31

32

33

34

35

36

37

38

39

40

41

42

43

44

45

46

47

48

49

50

51

52

53

Tropical deciduous forests (TDFs) are typically found in climates characterized by alternating dry and rainy seasons (Olson et al., 2001) and low seasonal temperature variability (U.S. DOE, 2012). As a major forest type in the tropics, TDFs play an important role in regulating the dynamics of the tropical carbon cycle (Kaewthongrach et al., 2020; Portillo-Quintero et al.,

2015; Wohlfart et al., 2014). However, they have been largely influenced by climate change and land use changes in Mainland Southeast Asia (MSEA) (Wohlfart et al., 2014). Projected global warming and shifts in precipitation patterns to more extreme events and severe droughts could lead to a significant amount of carbon emissions from the MSEA region into the atmosphere (Kondo et al., 2018; Liu et al., 2017; Manomaiphiboon et al., 2013). In addition, the MSEA has become a global hotspot of deforestation for conversion to agriculture (Grogan et al., 2019; Hurni and Fox, 2018). Because of increased global market incentives and economic profits, tree-based crops, especially rubber (*Hevea brasiliensis*) plantations, have been established across the region (Ahrends et al., 2015; Grogan et al., 2019; Kaewthongrach et al., 2020) threatening TDFs, which have low structural complexity and biomass to clear and comfortable environmental conditions to develop plantations (Portillo-Quintero et al., 2015). Assessing the impacts of these disturbances on forest production is essential for ensuring productive agriculture and understanding the terrestrial carbon budget, yet relevant studies are still limited in this region.

The eddy covariance (EC) technique is commonly used to estimate ecosystem gross primary production (GPP) for investigating ecosystem-atmosphere interactions (Baldocchi, 2003; Reichstein et al., 2013) and validating land surface models (Baldocchi, 2020; Thorn et al., 2015). Based on the EC technique, a study found a mean ± standard error annual GPP of 2156 ± 186 g C m⁻² yr⁻¹ of two evergreen forests and one plantation forest in the tropical region of China (Chen et al., 2019). In contrast, annual GPP in two primary evergreen forest in Thailand and Malaysia was 3200 – 3960 g C m⁻² yr⁻¹ (Adachi et al., 2011). A 33-year-old rubber plantation showed significantly higher carbon sequestration (790 g C m⁻² yr⁻¹) than a primary evergreen forest (359 g C m⁻² yr⁻¹) in Yunnan, China, while this result does not mean rubber plantations can offset carbon release caused by deforestation since the whole life cycle of the forests is not captured (Song et al.,

2014). The observations at a rubber flux site in Hainan Island, China, indicated the vulnerability of rubber GPP to the flash drought varied across the seasons (Wei et al, 2022). A TDF site in MSEA showed a 9.6% decrease of GPP by the prolonged drought in 2015/2016 (Kaewthongrach et al., 2020). Based on three forest sites, Wang et al. (2022) found a slightly higher annual GPP in a young secondary deciduous forest than rubber plantations and different forest responses to this prolonged drought across the seasons. Different tropical natural forests also had distinct strategy (i.e., water stress or light benefits) on carbon assimilation to adapt to limited water availability under dry conditions (Yang et al., 2022). Large uncertainties in carbon dynamics and responses to drought still exist due to complexity of stand age, tree density, and environmental conditions and the lack of long-term data and representative samples over space. At present, the distribution of EC flux towers is still sparse in the tropics, particularly in MSEA, which makes it difficult to examine forest GPP variations at a larger scale. Techniques that can be used to monitor the regional forest production and condition are thus urgently needed.

In recent years, satellite observations of solar-induced chlorophyll fluorescence (SIF) have been widely used to estimate vegetation photosynthesis due to its direct link to vegetation dynamics of photosynthesis (Frankenberg et al., 2011; Xiao et al., 2019). Satellite observed SIF from the Greenhouse Gases Observing Satellite (GOSAT, 10 km in diameter) and the Global Ozone Monitoring Experiment 2 (GOME-2, 80×40 km²) has shown strong empirical relationships to GPP estimates at large scales (Guan et al., 2016; Joiner et al., 2014). The release of the finer-resolution (1.3 × 2.25 km²) SIF products from NASA's Orbiting Carbon Observatory-2 (OCO-2) satellite makes it possible to directly link SIF to EC-based GPP (GPP_{EC}) at a finer scale (Frankenberg et al., 2014; Li et al., 2018a, 2018b; Sun et al., 2017; Verma et al., 2017; Wood et al., 2017). To overcome the spatial gaps and low temporal resolution of OCO-2 SIF, global

contiguous gridded SIF datasets with finer resolution (0.05°) such as GOSIF (Li and Xiao, 2019) and $\overline{SIF}_{oco2\ 005}$ (Yu et al. 2019) were reconstructed by using machine learning methods. Moreover, the physiological link between SIF and GPP also implies the ability of SIF to detect the impact of droughts on vegetation photosynthesis and its rapid responses to water and heat stresses at a regional scale. GOME-2 SIF revealed drought onset mechanisms in the US (Sun et al., 2015) and showed different responses of mixed forest, crops and grasslands to the 2010 Russian drought (Yoshida et al., 2015). Under heat stress, winter wheat in India had a larger decrease in SIF compared to normalized difference vegetation index (NDVI) and the enhanced vegetation index (EVI) (Song et al., 2018) and OCO-2 SIF showed a more significant and earlier response of Australian dryland vegetation than GOME-2 SIF (Qiu et al., 2020). Additionally, GOSIF captured ecosystem responses to soil moisture anomalies during the 2018 US drought (Li et al., 2020) and showed a two-month lag to soil moisture anomaly in northern China (T. Zhang et al., 2023). In MSEA, Qian et al. (2019) found a widespread SIF decline due to the prolonged drought during the 2015/2016 El Niño, while the regional drought impacts on TDFs, which are important to the carbon cycle and highly mixed with other land uses (Siyum, 2020), have never been investigated. It is necessary to examine the performance of SIF products for assessing photosynthesis variations in response to drought in TDFs before considering their usage at a continental scale.

100

101

102

103

104

105

106

107

108

109

110

111

112

113

114

115

116

117

118

119

120

121

122

Uncertainties exist in the SIF-GPP relationship due to the lack of clear mechanistic explanation of the relative contributions of canopy structural and physiological effects to SIF and how they relate to photosynthetic light use efficiency (LUE_p), especially under drought (Zhang et al., 2020). Light energy absorbed by a leaf that is allocated to photosystem II (PSII) is subject to competitive dissipation via three pathways: photochemistry, non-photochemical quenching (NPQ) and fluorescence (Govindjee, 1995). Drought stress can reduce carbon assimilation by decreasing

stomatal conductance and thus CO₂ availability within leaves (Chaves, 1991; Flexas et al., 2004), or changing photosynthetic metabolism with the increase of heat dissipation in the form of non-photochemical quenching (Müller et al., 2001; Tezara et al., 1999). Additionally, drought stress can cause long-term changes in canopy structure, such as leaf area index (LAI), leaf angle distribution and leaf clumping, all of which affect both canopy light absorption and scattering of the emitted SIF (Parazoo et al., 2020). To better estimate the overall canopy structural effects, NIR_v was recently developed and found to have strong correlations to SIF and GPP for various biomes (Badgley et al., 2019, 2017; Wang et al., 2020). Therefore, disentangling the relative contributions from different components (canopy structure or physiology) to the integrated canopy information under various environmental conditions will improve our mechanistic understanding of SIF-GPP relationship.

Based on multiple remotely sensed photosynthesis proxies, including native OCO-2 SIF (SIF_{native}), GOSIF, $\overline{SIF}_{oco2_005}$, NDVI, EVI, and NIR_v, and daily GPP_{EC} from two mature rubber plantations and one young natural forest sites, this study aims to: (1) evaluate the performances of remotely sensed proxies in estimating forest GPP and stress induced by the prolonged and severe drought in 2015/2016; (2) disentangle the structural and physiological proportions of SIF to GPP; and (3) investigate the spatial pattern of forest photosynthesis in MSEA and different forest responses to drought at a regional scale.

2 Materials and Methods

2.1 Study Region and Ground-based GPP Estimates

MSEA is a tropical region characterized as monsoonal with a mean annual air temperature of 25 ± 2 °C (Ian et al., 2020). There is a pronounced rainy season (May-October) influenced by the Southwest Asian monsoon (Chabangborn, 2014). We obtained the 200-m land cover map of

MSEA in 2015, which was developed based on Landsat and Moderate Resolution Imaging Spectroradiometer (MODIS) legacy collections and machine learning methods (Saah et al., 2020), from the Servir-Mekong's Regional Land Cover Monitoring System (https://www.landcovermapping.org/en/landcover/). According to this map, the dominant land cover types in MSEA are cropland (37%), natural evergreen forest (25%), natural deciduous forest (14%) and recently increased plantation forest (18%).

146

147

148

149

150

151

152

153

154

155

156

157

158

159

160

161

162

163

164

165

166

167

168

We obtained ground-based GPP estimates from EC flux towers in three TDFs, including two mature rubber monocultures and one secondary natural forest, along the Gulf of Thailand (Fig. 1). The southern rubber (SR) site was in a traditional rubber plantation area in southern Thailand where the weather condition is classified under the Köppen system as the tropical equatorial climate. The northern rubber (NR) site was 607 km north of the SR site, an area regarded as marginal for rubber growth owing to lower precipitation (Table 1). in the tropical savanna climate. In the same climate, the natural forest (NF) site was covered by a secondary-growth young, dry dipterocarp forest dominated by deciduous or semi-deciduous tree species from the Dipterocarpaceae family (Kaewthongrach et al., 2019). Dipterocarp forest is a widely distributed forest type over the mainland but has been increasingly threatened by deforestation and plantation expansion in past decades (Wohlfart et al., 2014). The NF is dominated by deciduous or semideciduous tree species, mainly from the Dipterocarpaceae family (Kaewthongrach et al., 2019). In this forest, leaf senescence typically occurs between December and February, and the emergence of new leaves in March-April (Kaewthongrach et al., 2020, 2019), while in rubber tree plantations defoliation and refoliation generally occur in January and February-March, respectively (Wang et al., 2022; Xiao et al., 2021). The two rubber sites were surrounded by other similar rubber tree plantations and their canopies were significantly higher than those at the NF site (Table 1).

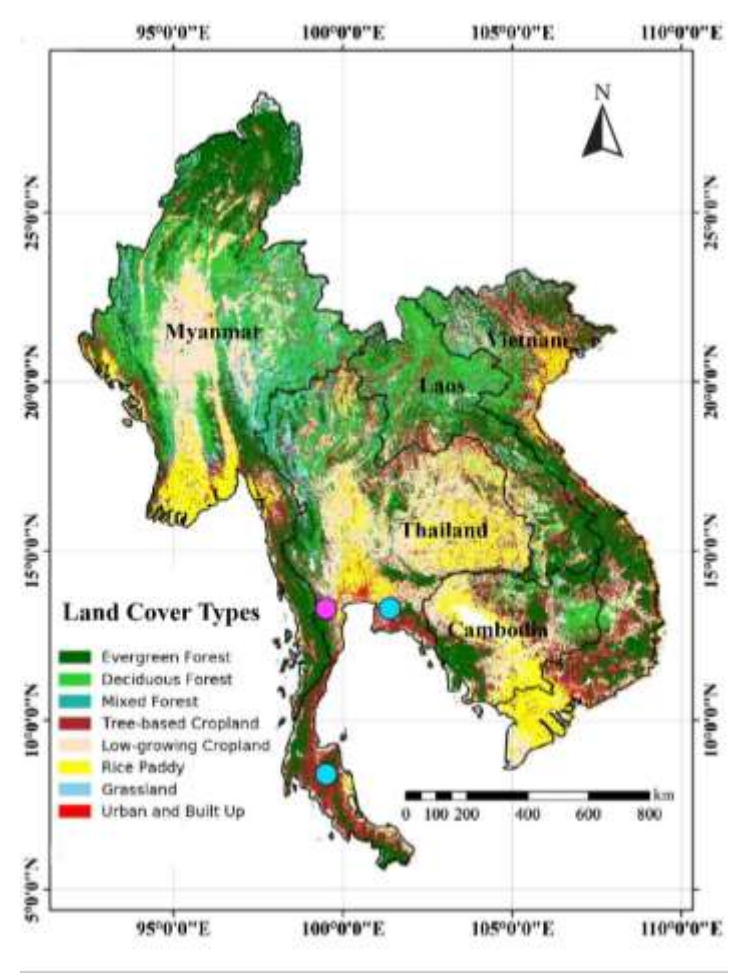


Figure 1. Land cover map of the Mainland Southeast Asia (MSEA) and the location of three eddy covariance (EC) flux sites selected in this study. The map was obtained from Servir-Mekong (https://www.landcovermapping.org/en/landcover/). Blue circles: the Northern Rubber (NR) and the Southern Rubber (SR) sites. Cyan circle: the Natural Forest (NF) site.

Table 1. General information of the canopy, including canopy height (m) in the year of observation, tree age, occupied area, dominant species, mean annual temperature (MAT), mean annual precipitation (MAP), 5-cm soil moisture (SM), and observation period in the study period at the northern rubber site (NR), the natural forest site (NF), and the southern rubber site (SR), respectively.

| Site | Northern Rubber (NR) | Natural Forest (NF) | Southern Rubber (SR) |
|--------------------|----------------------|---------------------|----------------------|
| Position | 13°34'N, 101°28'E | 13°35'N, 99°30'E | 8°19'N, 99°35'E |
| Elevation (a.s.l.) | 69 m | 118 m | 200 m |
| Canopy height (m) | 20.0 (2013) | 7.0 (2015) | 22.1 (2019) |

| Age (years) | 27 | 17–19 | 19 |
|--------------------------------------|--------------------|--|--------------------|
| Area (ha) | 8 | 89 | 16 |
| Dominant species | Hevea brasiliensis | Dipterocarpus obtusifolius Teijsm. Ex Miq, Shorea siamensis Miq., Shorea obtusa Wall., Shorea roxburghii G. Don, and Sindora siamensis Teijsm. & Miq | Hevea brasiliensis |
| MAT (°C) | 27.42 ± 1.68 | 27.28 ± 2.15 | 26.43 ± 1.07 |
| MAP (mm) | 1312 ± 519 | 1055 ± 192 | 3744 ± 463 |
| SM (m ³ m ⁻³) | 0.20 ± 0.02 | 0.08 ± 0.01 | 0.33 ± 0.01 |
| Observation period | 2015 – 2018 | 2015 – 2017 | 2017 – 2018 |

GPP was inferred by partitioning NEE using the night-time based (Reichstein et al., 2005) and day-time based (Lasslop et al., 2010) methods. To match the temporal resolution of OCO-2 SIF products, the daily GPP data smoothed using a 16-day moving average for the days of SIF products were selected to detect the daily SIF-GPP relationships. Additional site information and details on how GPP was derived from the EC measurements can be found in Wang et al., (2022).

2.2 OCO-2 SIF products

We used SIF products derived from observations made by the OCO-2 satellite. Far red SIF is retrieved from high resolution spectral measurements of the O2-A band using two solar Fraunhofer lines at 757 and 771 nm (Sun et al., 2018). The typical repeat cycle of OCO-2 is approximately 16 days, and the nominal spatial resolution is 1.3 km \times 2.25 km. We used the SIF Lite product (V8r), and calculated SIF_{native} for 2015 to 2018 at each site as the average of the SIF

at 757 nm and 1.5 times the SIF at 771 nm (Wood et al., 2017). Daily SIF_{native} was converted from the instantaneous observations by applying a daily correction factor which accounts for the variations of solar zenith angle and length of the day at each location (Sun et al., 2018). To ensure representativeness of the relationships at each site, we selected nadir SIF retrievals that were within a 50 km radius of the respective flux towers, and for which the pixel had 70% land cover similarity according to the 200-m land cover map from Servir-Mekong (Fig. 1).

The performance of daily SIF_{native} at each site was compared with two derivative gridded contiguous products (i.e., GOSIF and $\overline{SIF}_{oco2_005}$). GOSIF was developed by Li and Xiao (2019) and is produced at 0.05° and 8-day resolution (http://globalecology.unh.edu/). This product was generated by a Cubist regression tree model based on discrete OCO-2 SIF soundings, MODIS EVI, MODIS land cover type, and meteorological variables from MERRA-2. Global $\overline{SIF}_{oco2_005}$ product is produced at 0.05° and 16-day resolution using an artificial neural network on the SIF_{native}, MODIS reflectance and land cover (https://daac.ornl.gov/cgibin/dsviewer.pl?ds_id=1696). We extracted GOSIF and $\overline{SIF}_{oco2_005}$ at the pixel covering each flux tower during the period from 2015 to 2018.

2.3 MODIS Vegetation Indices

NDVI, EVI, and NIR_v were derived from the MODIS bidirectional reflectance distribution function (BRDF) corrected reflectance product (MCD43A4) at 500 m and 8-day resolution (Schaaf and Wang, 2015). To make VIs have comparable spatial resolution with the gridded SIF products, we averaged all pixels with high quality data within a $0.05^{\circ} \times 0.05^{\circ}$ window centered at each flux tower. To avoid the potential bias induced by inappropriate interpolation, we used the original temporal resolution for each satellite product in the analysis.

2.4 Drought Identification

213

214

215

216

217

218

219

220

221

222

223

224

225

226

227

228

229

230

231

232

233

234

235

The spatial pattern and duration of the drought 2015/2016 was determined using the monthly self-calibrating Palmer Drought Severity Index (scPDSI) for global land (https://crudata.uea.ac.uk/cru/data/drought/) from 1990 to 2018 at 0.5° spatial resolution based on the global Climate Research Unit (CRU) TS 4 dataset (Barichivich et al., 2021). The scPDSI is a variant of the PDSI (Palmer, 1965) that is calibrated to local climate and geographic information (Wells et al., 2004), and can thus be used to detect the long-term drought for different climate regimes (He et al., 2018; Trenberth et al., 2014; Van Der Schrier et al., 2013). According to Wells et al. (2004), the period with monthly scPDSI values less than -2 (sc-PDSI < -2) was considered under drought stress. The scPDSI values of the grid cell covering each site was extracted to determine the drought period and strength at the site scale. For the spatial analysis, we focused on the effects of long-term drought and only considered pixels with drought duration longer than 6 months. In addition, the standard anomalies of monthly temperature and precipitation from 1990 to 2018 at 0.5° spatial resolution from CRU TS v4 (Ian et al., 2020) were used to further interpret the drought event.

2.5 SIF-GPP relationships

The seasonal variations of daily SIF_{native}, GOSIF, $\overline{SIF}_{oco2_005}$, NDVI, EVI, NIR_v and GPP_{EC} were compared to examine the performance of SIF and other satellite products in monitoring forest GPP variations and drought effects. The t-test was used to determine statistical significance between drought and non-drought conditions. Even though the GPP product from the MODIS (Running et al., 2004) has a high spatial resolution (500 m), it was not included in this study because there was no significant correlation between this product and EC GPP at our sites (P-value >0.01).

To further explore the mechanism of forest SIF-GPP relationship and disentangle the structural and physiological contributions of SIF to GPP, we conducted a path analysis (Li, 1975) on the basis of the *LUE* model. According to the *LUE* model (Monteith, 1977, 1972):

$$GPP = APAR \cdot LUE_p \tag{1}$$

where APAR is the absorbed photosynthetically active radiation, which is the product of incident photosynthetically active radiation (PAR) and the fraction of the absorbed photosynthetically active radiation (fPAR). fPAR can be approximated by EVI (Xiao et al., 2004). LUE_p is the photosynthetic LUE of the canopy, and is a bulk term that represents many processes (i.e., photochemical, nonphotochemical, kinetic, physiological, and diffusive transport) (Gu et al., 2019). Similarly, SIF observed above the canopy is related to APAR and can be expressed as:

$$SIF = APAR \cdot \emptyset_F \cdot f_{esc} \tag{2}$$

Thus, GPP can be written as a function of SIF:

- where \emptyset_F is the quantum yield of SIF for the total canopy. f_{esc} is the escape probability of SIF photons that accounts for scattering and absorption of fluorescence photons within the canopy.
- LUE

$$GPP = \frac{LUE_p}{\phi_{F} \cdot f_{esc}} SIF$$
 (3)

 $\frac{LUE_p}{\emptyset_F \ f_{esc}}$ represents the physiological nonlinearity between LUE_p and \emptyset_F , resulting from the saturating light response of photosynthesis at high light as the carboxylation is limited by stomata and mesophyll diffusion while a stronger tendency of SIF to keep increasing due to a lower sensitivity of SIF to light and the compensating effect of NPQ and photochemistry (Gu et al., 2019). Eq. 3 indicates that GPP is determined by SIF and the nonlinear term of $\frac{LUE_p}{\emptyset_F \ f_{esc}}$. Since LUE_p varies with environmental conditions, and also with the canopy structure and illumination-viewing

geometries via f_{esc} (Hao et al., 2021), the canopy structure effect on LUE_p is excluded by $\frac{LUE_p}{f_{esc}}$ and linked only to the term of SIF in Eq. 3. According to Zeng et al. (2019), except for very low fractional vegetation cover, f_{esc} can be approximated as:

$$f_{esc} \approx \frac{NIR_v}{fPAR} \tag{4}$$

Then, according to Eq. (2) and Eq. (4), SIF can be written as:

$$SIF \approx PAR \cdot \emptyset_F \cdot NIR_v \tag{5}$$

where NIR_v describes the integrated canopy structure effects of absorption and scattering (Dechant et al., 2022, 2020).

In path analysis, direct effect refers to the relationship between two adjacent variables and indirect effect refers to the relationship between two variables that is mediated by one or more intervening variables. We designed the paths according to Eq. 3 and Eq. 5: NIR_v, PAR and \emptyset_F first influence SIF variations, and then SIF and the physiological nonlinearity between LUE_p and \emptyset_F influence GPP variations. Based on the lavaan package (Rosseel, 2012) in R, the direct effects of NIR_v, PAR, and \emptyset_F on SIF, as well as the direct effects of SIF and $\frac{LUE_p}{\emptyset_F \cdot f_{esc}}$ on GPP were calculated by the standardized path coefficients in path analysis. The indirect effects of NIR_v PAR, and \emptyset_F on GPP via SIF were calculated by the product of the standardized coefficient between the corresponding factor and SIF and that between SIF and GPP, respectively.

2.6 Regional analysis

We first analyzed the spatial patterns of different remotely-sensed photosynthesis proxies and quantified their differences among multiple vegetation types in MSEA. Then, we examined the spatial changes (%) of these proxies induced by the prolonged drought for each pixel as the

difference between drought and non-drought conditions divided by the non-drought mean. To maintain the consistency between satellite products and their advantage of the relatively high spatial resolution, we used the aggregated 0.05° and monthly mean EVI, NIR_v, GOSIF, and $\overline{SIF}_{oco2_005}$, and the aggregated 0.5° and monthly mean SIF_{native}, for the spatial analysis. Only the pixels with the duration of drought (scPDIS<-2) longer than 6 months were considered to investigate the long-term drought impacts on different proxies among different vegetation types.

3 Results

3.1 Site-level relationships between GPP and remotely sensed photosynthesis proxies at the site scales

3.1.1 Seasonal variations

Daily variations of GPP_{EC} and different remotely sensed photosynthesis proxies were shown in Fig. 2. The three sites exhibited different seasonality of photosynthesis, with larger amplitude of GPP_{EC} and later dormancy period in the natural forest than in the rubber plantations. Overall, all the satellite products captured the seasonal cycles of photosynthesis in the TDFs and indicated significant linear relationships to GPP_{EC} ($R^2 > 0.42$, p-values < 0.05) with the equations and R^2 of the linear regression models shown in Fig. 2. However, the rubber plantations showed lower GPP_{EC} and SIF (Fig. 2a, 2c) while significantly higher VIs (i.e., NDVI, EVI and NIR_v) than the young natural forest (Fig. 2b, 2f), leading to the larger intercepts in the linear regression models of GPP_{EC} by VIs than SIF. In addition to the SIF (R^2 : 0.52 – 0.75), NIR_v (R^2 : 0.74 – 0.79) had substantially stronger correlations with GPP_{EC} than NDVI or EVI (R^2 : 0.42 – 0.51) did for the rubber plantations, where NDVI and EVI were more susceptible to saturation and exhibited less capacity to show the seasonal peak in the rainy seasons. This phenomenon also occurred in GOSIF even though it (R^2 : 0.59 – 0.75) outperformed $\overline{SIF}_{oco2_005}$ (R^2 : 0.55 – 0.63) and SIF_{native} (R^2 : 0.54 – 0.65) in detecting the seasonal variability of GPP_{EC}. For the young natural forest, NDVI and EVI

 $(R^2 > 0.82)$ had stronger temporal consistency with GPP_{EC} than NIR_v (R^2 =0.74) and SIF (R^2 : 0.52 – 0.71). Overall, NIR_v showed a strong and stable ability to estimate the seasonal variability of GPP_{EC} within the ecosystem and SIF, especially GOSIF, outperformed VIs to indicate the GPP_{EC} differences among multiple TDF ecosystems.

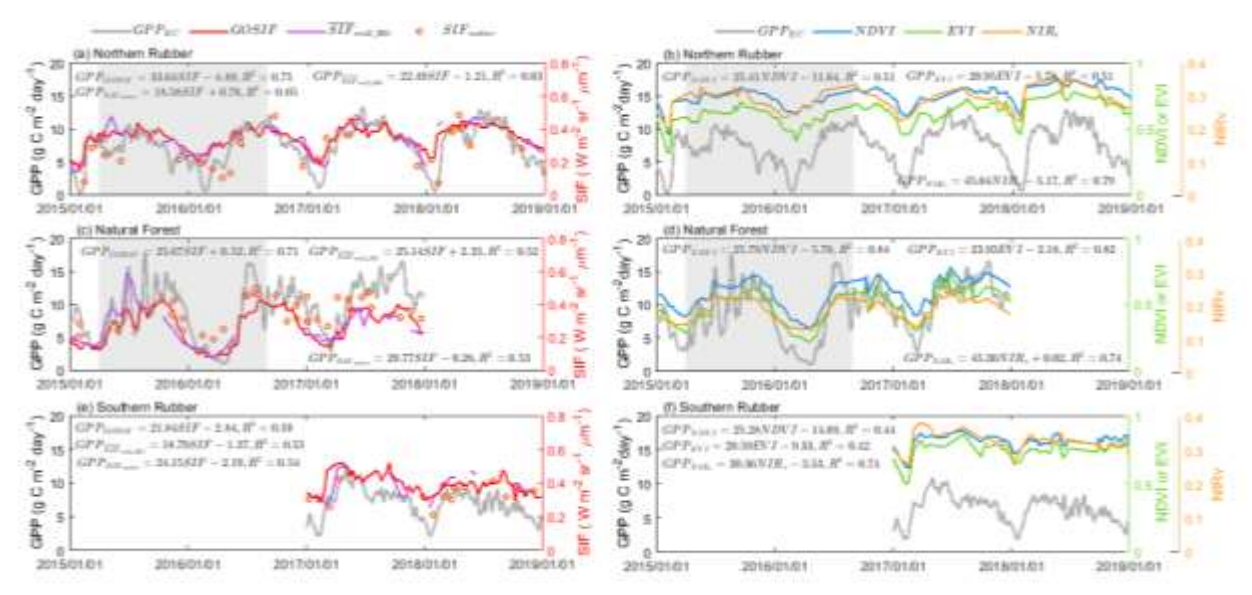


Figure 2. Time series of daily GPP_{EC} and GOSIF, $\overline{SIF}_{oco2_005}$, SIF_{native}, NDVI, EVI, and NIR_v from 2015 to 2018 at the Northern Rubber site (a,b), Natural Forest site (c,d), and the Southern Rubber site (e,f). Shaded areas represent the prolonged drought period from April 2015 to August 2016, which was determined by sc-PDSI < -2 based on the long-term CRU dataset.

3.1.2 Performance of modeled GPP in estimating drought effects

A strong El Niño event (Burton et al., 2018) caused the NR and NF sites to suffer from prolonged and severe drought from April 2015 to August 2016 (Fig. 2). We used the modeled GPP from the linear regressions (Fig. 2) to examine the performance of different satellite products for estimating the drought effects on photosynthesis (Fig. 3). GPP_{EC} in the dry season and the rainy season showed a significant (t-test, p-value < 0.05) decrease (18% and 10% at the NR site, and 33% and 18% at the NF site, respectively) by drought, which was successfully captured by SIF (Fig. 3a, 3b). At the NR sites, particularly in the rainy season, the modeled GPP from SIF except for SIF_{native} better estimated the drought-induced reduction (by 7%) than GPP_{EVI} and GPP_{NIRv} (by 1%). The

sparse observations of SIF_{native} when high GPP_{EC} occurred resulted in underestimation of GPP in the rainy season. At the NF site, modeled GPP from EVI (2.24 g C m⁻² day⁻¹) and NIR_v (1.29 g C m⁻² day⁻¹) performed better in detecting the difference of GPP_{EC} (2.30 g C m⁻² day⁻¹) between two drought conditions than that from SIF (-0. 25 – 0.31 g C m⁻² day⁻¹) in the rainy season. The enlarged inter-quartile ranges of NF GPP_{EC} due to the drier condition were successfully captured by GPP_{GOSIF}, GPP_{EVI} and GPP_{NIRv}. At the SR site, we had only two years of tower observations (2017-2018) during non-drought condtions when the SR GPP_{EC} amplitude was obviously less than that at the NR site. The slight difference of mean GPP_{EC} (1.64 g C m⁻² day⁻¹) between two seasons was better detected by GPP_{GOSIF} (1.01 g C m⁻² day⁻¹) and GPP_{SIF005} (1.40 g C m⁻² day⁻¹) than GPP_{EVI} (0.86 g C m⁻² day⁻¹) and GPP_{NIRv} (0.83 g C m⁻² day⁻¹).

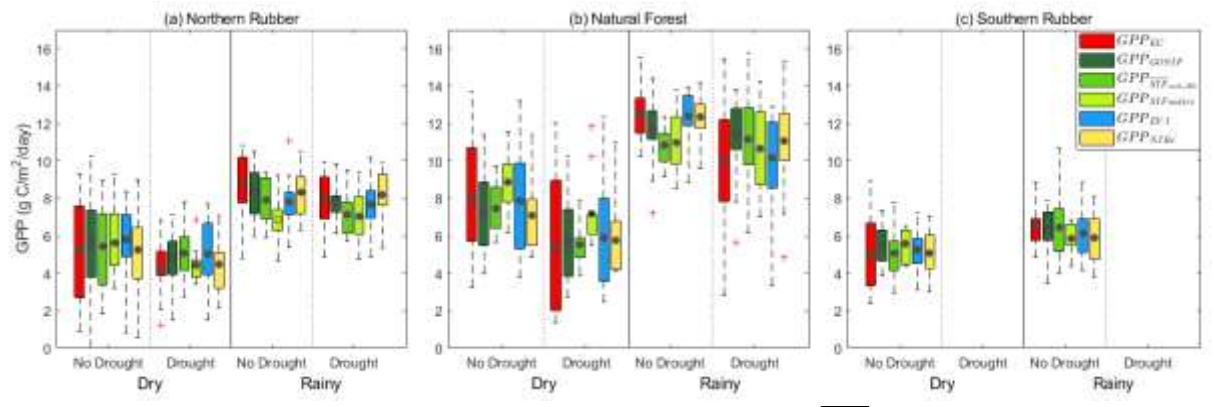


Figure 3. Boxplots of daily GPP_{EC} and modeled GPP by GOSIF, $\overline{SIF}_{oco2_005}$, SIF_{native}, NDVI, EVI, and NIR_v under non-drought and drought conditions in dry and rainy seasons at the Northern Rubber site (a), Natural Forest site (b), and Southern Rubber site (c). The boxplots depict the 25th and 75th percentiles (edges of the box), the maximum and minimum GPP (whiskers), the outliers (red plus) and the mean (central circle). The filled circle represents no significant difference between GPP_{EC} and the corresponding modeled GPP (t-test, p-value>0.05).

3.1.3 Contribution of canopy structure in SIF-GPP relationship

Significant linear correlations were found between daily GPP_{EC} and SIF products, as well as between SIF products and NIR_v at all three study sites (Fig. 4). The higher R² (>0.5) suggests a dominant role of SIF to explain GPP variations and that of NIR_v to explain SIF. To better understand the SIF-GPP relationships, we used path analysis to compare the effects of NIR_v and

other related factors (i.e., ϕ_F , PAR, and $\frac{LUE_p}{\phi_F f_{esc}}$) in Fig. 5. Despite the presence of physiological nonlinearity between LUE_p and ϕ_F at the seasonal scale, SIF performed well in estimating GPP variations with much higher effects (0.7-0.88) than the nonlinearity term (0.35-0.58). Consistent with Fig. 4, the higher indirect effects of NIR_v (0.59-0.81) than PAR (0.01-0.11) and ϕ_F (0.27-0.41) in path analysis revealed the primary contribution of canopy structure to link SIF and GPP at the NR and the NF sites (Fig. 5a, 5b). At the SR sites, GPP and NIR_v had less variability (Fig. 2) in the humid and warm condition, accompanied by an increased effect of $\frac{LUE_p}{\phi_F f_{esc}}$ (Fig. 5c). Even though the canopy structure is still a major factor to influence GPP via SIF, the indirect effects of PAR (0.24-0.48) and ϕ_F (0.57-0.63) became stronger at the SR site compared to the two northern sites.

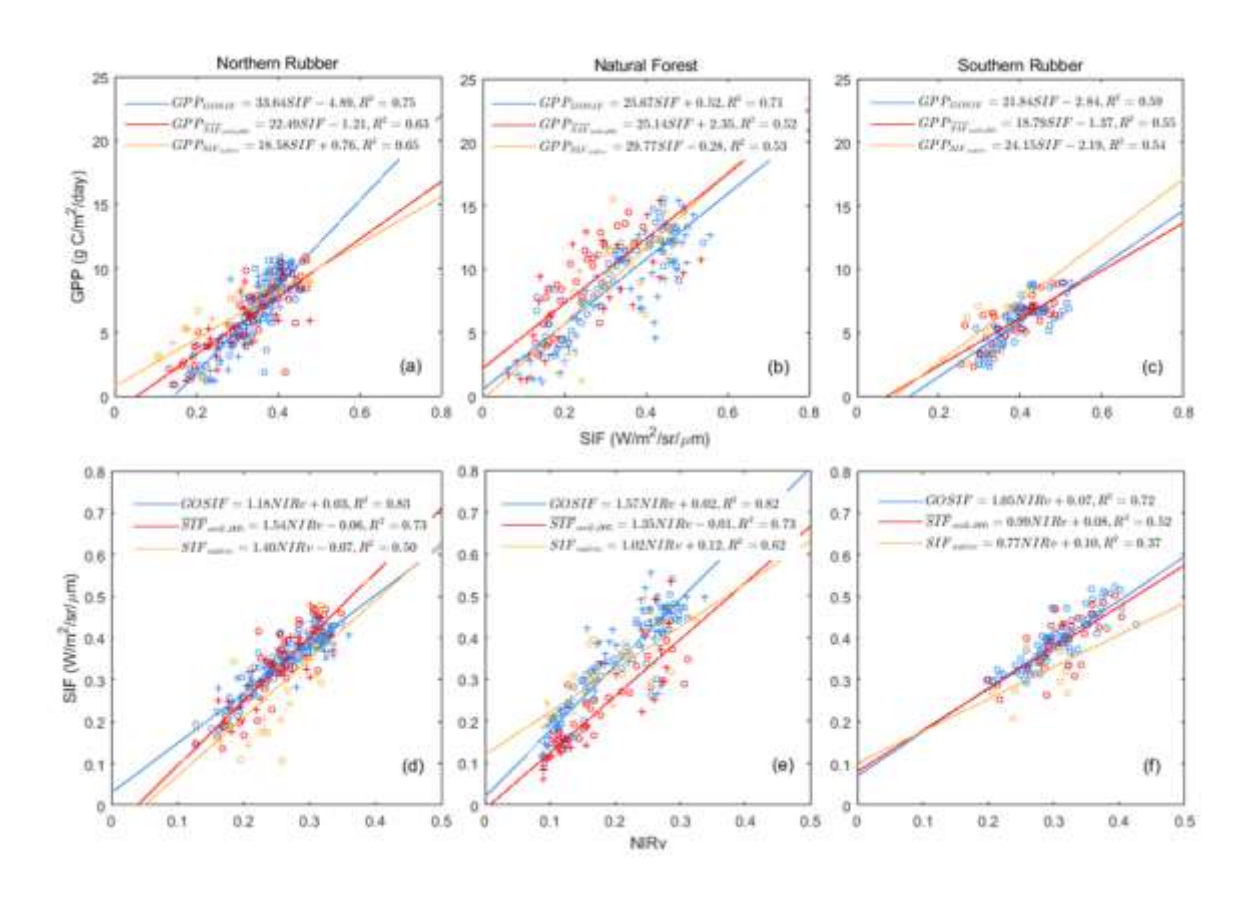


Figure 4. Linear relationships between daily GOSIF, $\overline{SIF}_{oco2_005}$, SIFnative, and GPP, and that between GOSIF, $\overline{SIF}_{oco2_005}$, SIF_{native}, and NIR_v at the Northern Rubber site (a,d), Natural Forest site (b,e), and the Southern Rubber site (c,f). Daily values in non-drought (o) and drought (+) conditions are shown separately.

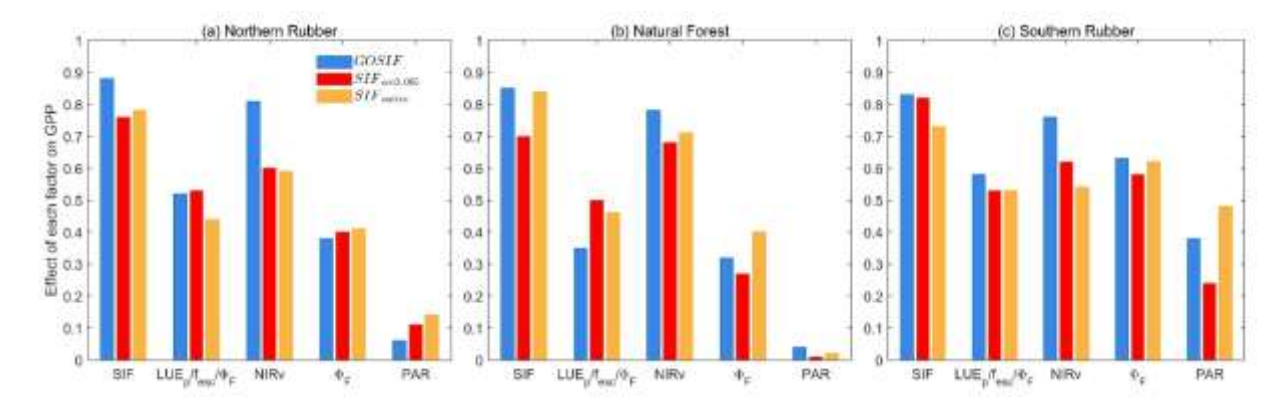


Figure 5. Comparison of the direct effects of SIF and $\frac{LUE_p}{\phi_F f_{esc}}$, and the indirect effects of NIR_v, ϕ_F , and PAR on GPP_{EC} via SIF based on path analysis at the Northern Rubber site (a), Natural Forest site (b), and Southern Rubber site (c).

3.2 Remotely sensed photosynthesis at the regional scale

3.2.1 Spatial pattern of vegetation photosynthesis

The significant linear relationships between the satellite products and GPP at the site-level validate the usage of SIF and VI as photosynthesis proxies. At the regional scale, all the satellite products indicated that tropical forests had higher photosynthesis than croplands (Fig. 6) which are mainly located in the middle, northwest and northeast of MSEA (Fig. 1). Compared to other satellite products, mean EVI was apparently larger in the evergreen forest (0.78), the natural deciduous forest (0.69) and plantation forest (0.65) (Fig. 6f). Taking the two forest areas where the rubber sites were located as an example, both SIF and NIR $_{v}$ exhibited lower photosynthesis in the evergreen forest than in their adjacent plantation forest in these areas (shown by the black dashed-line boxes in Fig. 6a, b, c, e), which was opposite to EVI results (Fig. 6d). The difference between natural deciduous forest and plantation forest was positive in EVI (0.04) but not significant (t-test, p-value >0.05) in NIR $_{v}$ and GOSIF and was negative in $\overline{SIF}_{aco2_005}$ (-0.04) and

SIF_{native}, (-0.06) (Fig. 6f). Mean SIF for the forests sequentially decreased from GOSIF to $\overline{SIF}_{oco2\ 005}$ to SIF_{native}.

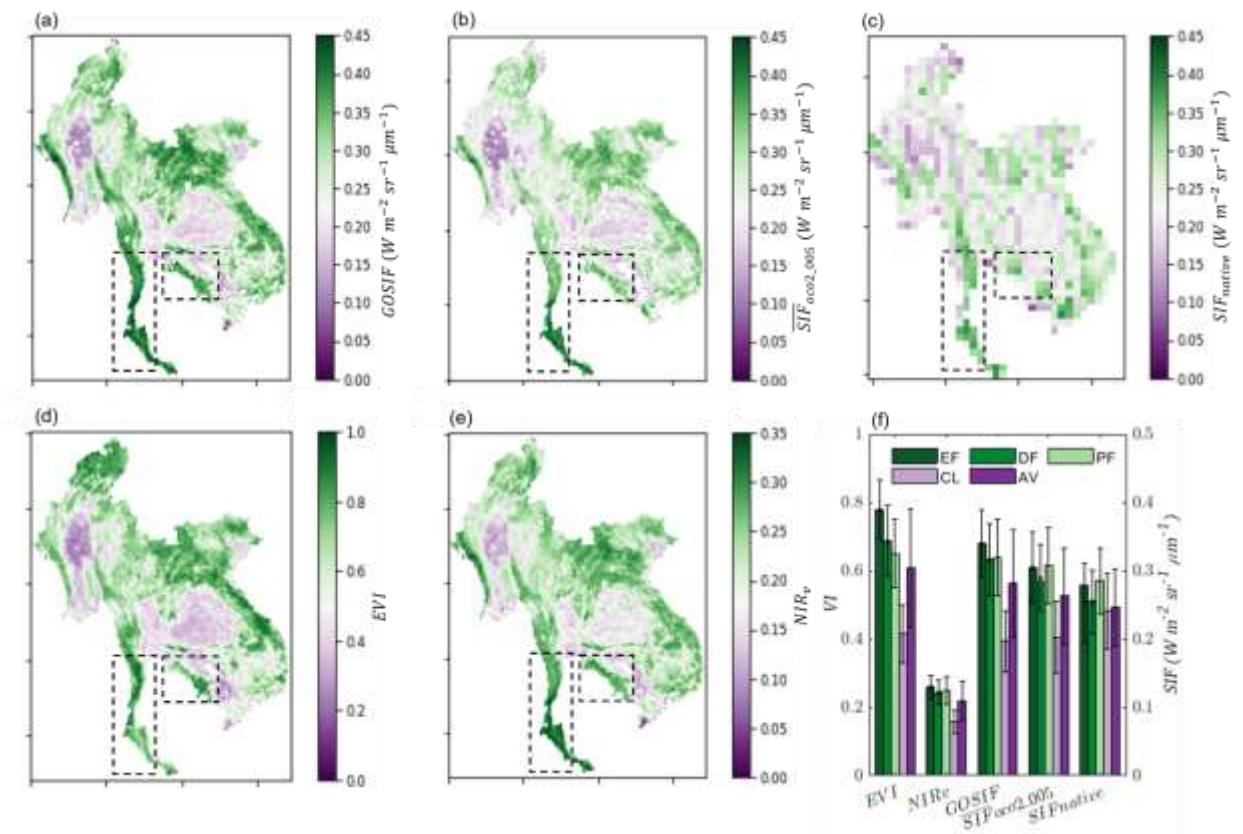


Figure 6. Spatial patterns of averaged GOSIF (a), $\overline{SIF}_{oco2_005}$ (b), SIF_{native} (c), EVI (d), and NIR_v (e) from August 2014 to August 2018 in MSEA, and their mean (+/- one standard deviation) for different vegetation types (f), including natural evergreen forest (EF), natural deciduous forest (DF), plantation forest (PF), cropland (CL), and all vegetation types (AV). Black dashed-line boxes highlight the forest areas with different spatial patterns between EVI and other proxies.

3.2.2 Response of vegetation to drought

According to scPDSI, the prolonged drought period occurred from September 2014 to August 2016, with significantly lower precipitation and higher temperature over the region (Fig. 7a). The maximum negative standardized anomalies (less than -1.5) of precipitation occurred in the eastern MSEA (Fig. 7b). The positive temperature anomalies were substantial over the most region, especially in North Thailand with standardized anomalies of up to 1.5 (Fig. 7c). As a result,

a large region of MSEA from northwest to southeast suffered from the prolonged drought (Fig. 7d).

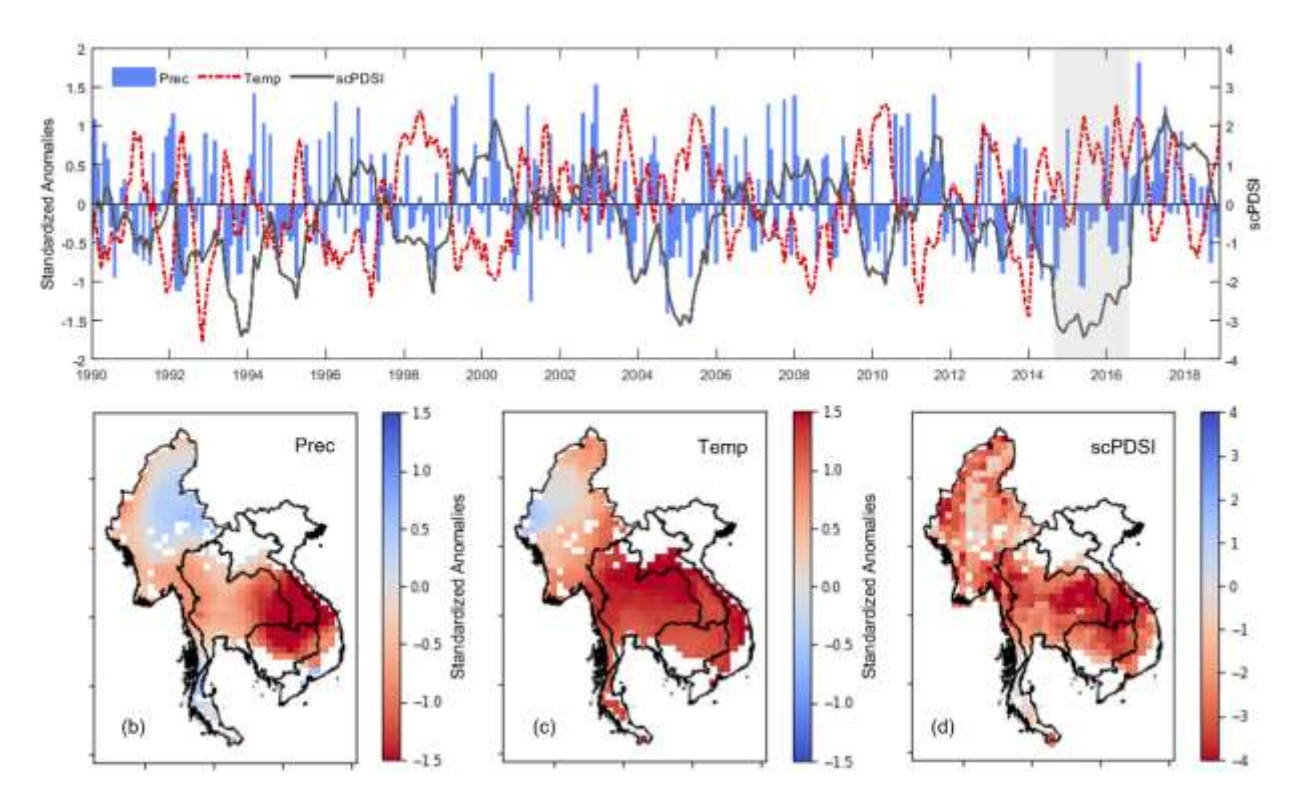


Figure 7. Spatiotemporal distributions of drought. (a) monthly standard anomalies (SA) of precipitation (Prec), temperature (Temp), and monthly scPDSI from 1900 to 2018. Shaded area represents the prolonged drought period from September 2014 to August 2016 (determined by scPDSI < -2). The spatial pattern of SA of (b) Prec, (c) Temp, and (d) scPDSI, respectively, in drought relative to the means during the reference period (1900 – 2018). We only considered the pixels with drought (scPDSI < -2) duration longer than 6 months to assess the long-term drought effects on vegetation.

Both VI and SIF showed negative changes in response to the drought (Fig. 8). The proxies decreased by over 15% in central Myanmar, Central Thailand, and North Cambodia, which were mainly covered by cropland, natural deciduous forest or plantation forest (Fig. 1). In contrast to GOSIF and SIF_{native}, $\overline{SIF}_{oco2_005}$ indicated less drought impact in MSEA and a positive change in Northeast Thailand (Fig. 8d). Furthermore, the suppression in response to drought varied among different vegetation types (Fig. 9). Evergreen forest suffered from the least impact during the

prolonged drought, with an averaged change of photosynthesis proxy from -2% (EVI) – -6% $(\overline{SIF}_{oco2_005})$. In contrast, natural deciduous forest and plantation forest were more vulnerable to the drought, and the corresponding averaged declines were from -3% $(\overline{SIF}_{oco2_005})$ to -8% (GOSIF) and from -3% $(\overline{SIF}_{oco2_005})$ to -9% (SIF_{native}), respectively. The cropland suppression exhibited the largest differences among multiple proxies, from 2% $(\overline{SIF}_{oco2_005})$ to 10% (GOSIF). For all the vegetation types, EVI and NIR_v decreased by 6% and SIF decreased by 3% – 9%. The magnitude of averaged $\overline{SIF}_{oco2_005}$ change (from -2% to -3%) was much smaller than that of GOSIF (from -4% to -10%) and SIF_{native} (from -4% to -9%), while the variability of SIF_{native} change (SD: 7% – 10%) was significantly larger than that of other proxies (SD: 1% – 7%) among different vegetation types.

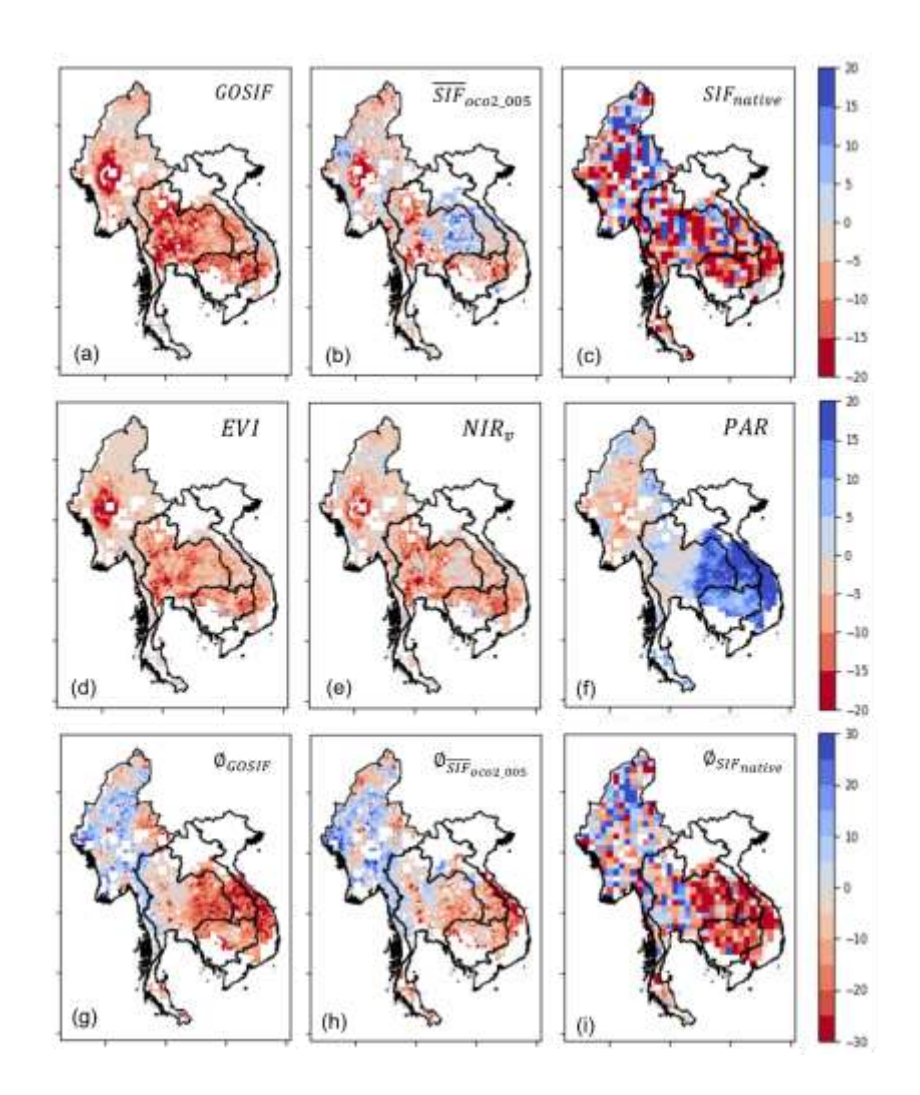


Figure 8. Spatial patterns of changes (%) of GOSIF (a), $\overline{SIF}_{oco2_005}$ (b), SIF_{native} (c), EVI (d), NIR_v (e), PAR (f), \emptyset_{GOSIF} (g), $\emptyset_{\overline{SIF}_{oco2_005}}$ (h), and $\emptyset_{SIFnative}$ (i) by drought (September 2014 – August 2016) compared to non-drought condition (September 2016 – August 2018). We only considered the pixels with drought (scPDSI < -2) duration longer than 6 months to assess the long-term drought effects on vegetation.

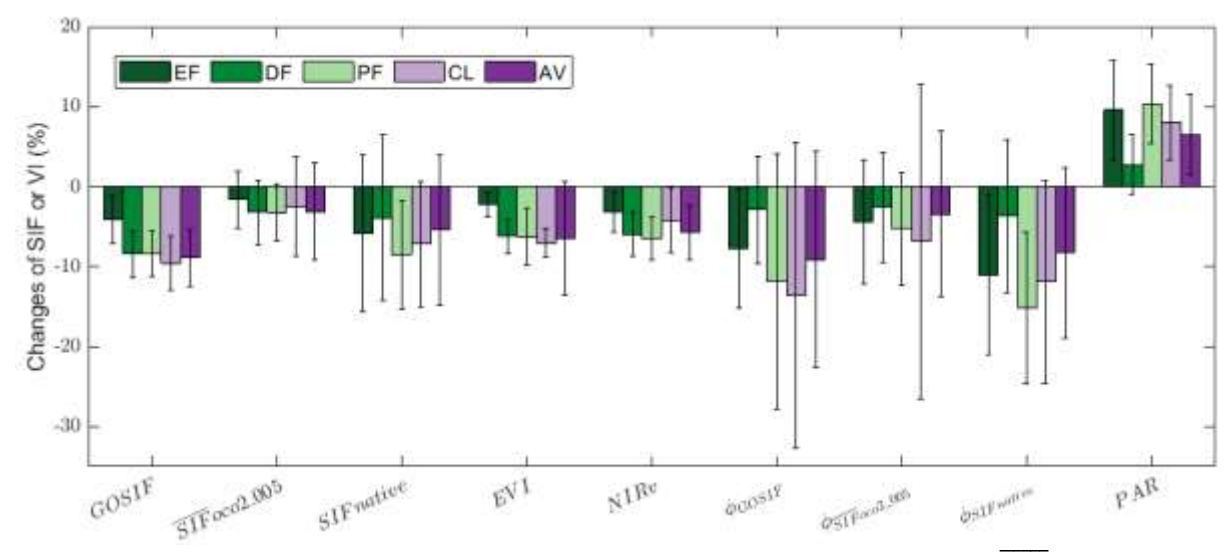


Figure 9. Mean (+/- one Standard Deviation, SD) of changes (%) of GOSIF, $\overline{SIF}_{oco2_005}$, SIF_{native} \emptyset_{GOSIF} , $\emptyset_{\overline{SIF}_{oco2_005}}$, $\emptyset_{SIFnative}$, EVI, NIR_v, and PAR by drought (September 2014 – August 2016) compared to non-drought condition (September 2016 – August 2018) in different vegetation types including natural evergreen forest (EF), natural deciduous forest (DF), plantation forest (PF), cropland (CL), and all vegetation types (AV).

Furthermore, the spatial patterns of the PAR and \emptyset_F changes induced by drought were shown in Fig. 8f-8i. Inversely related to the spatial pattern of precipitation anomalies, PAR showed a large increase (more than 15%) in the eastern MSEA likely due to the less cloud coverage while a slight decrease in Myanmar in response to drought. Correspondingly, all the \emptyset_F estimates had a large decrease in the eastern MSEA. The averaged changes of \emptyset_F induced by drought (from -3% to -15%) were more substantial than those of SIF and VI except for natural deciduous forest (Fig. 9). Natural deciduous forest was mainly located in the northern MSEA (Fig. 1) with less precipitation anomalies (Fig. 7b) and PAR anomalies (Fig. 8f) under drought. Consistent with SIF products, drought-induced \emptyset_F changes calculated by $\overline{SIF}_{oco2_005}$ (from -3% to -7%) were less than \emptyset_{GOSIF} (from -3% to -14%) and $\emptyset_{SIF_{nattive}}$ (from -4% to -15%). The variabilities of \emptyset_F changes (SD: 7% – 19%), however, were significantly larger than SIF changes (SD: 3% – 10%), especially in cropland.

4 Discussion

447

448

449

450

451

452

453

454

455

456

457

458

459

460

461

462

463

464

465

466

467

468

469

4.1 Relationships between tower GPP and remotely sensed vegetation proxies

Consistent with previous studies related to other forest types in different latitudes (Shekhar et al., 2022; Lu et al., 2018; Zuromski et al., 2018), the linear SIF-GPP relationships at the three forest sites varied across SIF datasets, different forest characteristics and environmental conditions (Fig. 2). As SIF is more linked to the vegetation dynamics of photosynthesis than the remotely sensed vegetation greenness, it was expected that the SIF products indicated stronger correlations with GPP (R^2 : 0.54 – 0.75) in the two rubber plantations compared to NDVI and EVI (R^2 : 0.42 – 0.51). Particularly, GOSIF outperformed $\overline{SIF}_{0co2,005}$ and SIF_{native} in estimating the seasonal variations of GPP. In addition to MODIS reflectance, GOSIF uses meteorological data in its development and has higher temporal resolution compared to $\overline{SIF}_{oco2\ 005}$. Therefore, GOSIF likely includes more information on physiological response to the environmental factors besides the structural response depicted by MODIS reflectance. Additionally, the saturation of NDVI and EVI was significant at the rubber sites with high values of LAI (Wang et al., 2022), resulting in their lower relationships to GPP (\mathbb{R}^2 : 0.42 – 0.51). The long time (March – September) of the fully expanded leaf stage of rubber trees (Chayawat et al., 2019) could also cause the less variability of greenness during this period. Furthermore, the large intercepts in the fitting models of NDVI and EVI would decrease the regression accuracy since a small bias could lead to a significant difference of GPP, particularly at the SR site. The greater intercepts of all the satellite vegetation proxies at the SR site than at the NR site were probably attributed to the higher soil moisture (Wang et al., 2022), and thus less foliage abscission in the dry season in the south (Table 1).

At the young NF site, however, VI showed higher correlations to GPP than did SIF. Similar results were also found in the tropical dryland savannas (Wang et al., 2019). SIF products could

be restricted by the scale match or mismatch between flux tower footprint and OCO-2 footprint. The scale mismatch between SIF_{native} and the NF tower footprint could degrade the SIF-GPP relationship as the NF site that was located in the orbital gaps of OCO-2 (Wang et al., 2019). It is noted that NIR_v, designed to better characterize canopy structure, had an efficient and stable ability to estimate GPP_{EC} and even performed better than GOSIF for both the young NF and the mature rubber plantations (R² > 0.74). Compared with traditional VI, NIR_v has a more direct physical interpretation as it presents the proportion of NIR light reflected by vegetation canopy (Badgley et al. 2017), which minimizes the impacts of soil background and sun-canopy-sensor geometry (Badgley et al., 2019). The higher correlations between GPP_{EC} and NIR_v than between GPP_{EC} and SIF suggest the need for more high-resolution and good-quality SIF products for the ecosystem-scale GPP detection in the future.

Path analysis demonstrated the dominant role of canopy structure (NIR_v) on SIF-GPP relationship. Similar result was also found in the temperate crops (Dechant et al., 2022, 2020). NIR_v ($\approx fPAR \cdot f_{esc}$) describes the integrated canopy structure effects of absorption and scattering (Dechant et al., 2020). In addition to fPAR mainly controlled by LAI, NIR_v also relates to the canopy scattering via f_{esc} and suggests a possible effect of leaf angle distribution on LUE_p by modifying the fraction of sunlit and shaded leaves (Hao et al., 2021). As a tree species from humid tropics, mature rubber monocultures had taller and denser crowns than the NF. The individual rubber trees may tend to minimize foliage overlap by changing the leaf angle distribution from planophile during the green-up period to more erectophile as the canopy closes. Modeling and observations have shown that erectophile canopies have significant less variability of LUE_p with \emptyset_F and much lower f_{esc} than planophile canopies (Hao et al., 2021; L. He et al., 2018; Zeng et al., 2019), which could explain the significantly decreased NIR_v while relatively constant NDVI and

EVI at the end of each year at the NR and the SR sites (Fig. 2b, 2f). Although the canopy structure effect is important, the physiological effect (\emptyset_F) was likely to increase in a wetter condition (Fig. 5c) to adjust to some short-term changes in meteorological conditions, such as PAR, temperature, and soil moisture, when LAI was less varied after leaf became mature.

493

494

495

496

497

498

499

500

501

502

503

504

505

506

507

508

509

510

511

512

513

Furthermore, we highlight the different usage of NIR_v and SIF in estimating canopy structure and photosynthesis, separately, in the comparison among multiple forest types. The mature rubber plantations at the NR and the SR sites showed much higher EVI while comparable SIF and GPP_{EC} compared to the young NF. Similarly, the spatial pattern of remotely sensed variables exhibited higher VI (i.e., EVI and NIR_v) while lower SIF of natural deciduous forest than that of plantation forest (Fig. 7f). Additionally, both the natural deciduous forest and plantation forest had higher SIF, but lower EVI compared to evergreen forest. Consistently, the tropical evergreen forest in Amazon showed largely reduced photosynthesis but slightly increased canopy greenness during the extreme drought (Yang et al., 2018). The inconsistency between VI and SIF emphasizes the unique advantage of SIF to monitor vegetation photosynthesis. Besides, the widely used 500-m MODIS GPP product (MOD17A2) was not shown in this study since it had no significant correlations to GPP_{EC} at our three sites. Other studies also pointed out the limited performance of the MODIS GPP product in multiple biomes (Qiu et al., 2020; Sjöström et al., 2013; Wu et al., 2018) due to the limitations of the LUE model and inaccurate input parameters. The remotely sensed SIF and their global continuous products are recommended to improve the direct GPP detection from the ecosystem to the regional scale for MSEA where multiple forest types are highly mixed.

4.3 Drought effects

514

515

516

517

518

519

520

521

522

523

524

525

526

527

528

529

530

531

532

533

534

535

536

The prolonged and severe drought in 2015/2016 (Fig. 7) caused a large decrease of vegetation photosynthesis at the flux sites and in the spatial pattern of MSEA. At both the NR and the NF sites, the drought suppression on GPP was more significant in the dry season than in the rainy season (Fig. 3). Under drought stress, the response of canopy leaf angle distribution can be significant and affect LUE_p by modifying the fraction of sunlit and shaded leaves (Xu et al., 2021), while the LAI changes mainly control *fPAR* (Zeng et al., 2019). Consistently, the spatial patterns of SIF changes induced by drought was more like EVI and NIR $_{\rm v}$ rather than \emptyset_F and PAR (Fig. 8). Besides, drought can also affect photosynthesis through the physiological processes, including increasing NPQ, decreasing enzyme activity and stomatal conductance to prevent excessive energy and water loss (Blackman et al., 2009; Flexas et al., 2000; Xu et al., 2020). To detect the physiological response to water and heat stresses, prior research approximated the fluorescence yield emitted from the top of the canopy (SIF_{yield}) as $\frac{SIF}{APAR}$. These studies indicated that SIF_{yield} had a higher sensitivity to water condition changes (i.e., water stress and recovery) than SIF and that the response of SIF_{yield} to water stress agreed well with LUE_p (Li et al., 2022; Ma et al., 2023; Qian et al., 2019). Our study further excluded the scattering effect of canopy structure on the fluorescence escaped probability (f_{esc}) and directly estimated the fluorescence yield from all the leaves in the canopy $(\emptyset_F = \frac{SIF}{APAR \cdot f_{esc}} = \frac{SIF}{PAR \cdot NIR_v})$ according to Eq. 5. Consistent with SIF_{yield}, the \emptyset_F estimates exhibited similar spatial pattern of precipitation anomaly (Fig. 7b) with a significant decrease in the eastern MSEA under drought (Fig.7g-7i). While this negative effect of water stress was offset by higher PAR (Fig. 8f), resulting in the smaller change of SIF compared to \emptyset_F under water stress. This also explains why the remaining effect of SIF on GPP_{EC} related to canopy physiology and PAR, was relatively small and did not change significantly

between non-drought and drought conditions at both the NR and the NF sites. \emptyset_F estimates (Fig. 9) had large variabilities because \emptyset_F , as a function of SIF, NIR_v, and PAR, directly inherited the uncertainties of these remotely sensed variables.

537

538

539

540

541

542

543

544

545

546

547

548

549

550

551

552

553

554

555

556

557

558

559

Both SIF and VI decreased in different vegetation types under the prolonged drought. GOSIF and SIF_{native} outperformed EVI and NIR_v by exhibiting more significant change in response to drought, while $\overline{SIF}_{0c02\ 005}$ was less sensitive to drought and even showed an opposite pattern in the Northeast Thailand compared to the other satellite variables. Consistent with $\emptyset_{SIFnative}$, \emptyset_{GOSIF} and $\emptyset_{\overline{SIF}_{OCO2,005}}$ showed a similar spatial pattern to the precipitation anomaly, suggesting the capacity of SIF_{native} and its gridded SIF products in capturing the physiological response to drought compared to VI. We found three areas with large negative change of SIF induced by drought: central Myanmar, Central Thailand, and Northeast Cambodia. Under the prolonged drought, the Central Dry Zone of Myanmar exhibited the most significant decline (larger than 15%) across all the vegetation proxies. Though being a primary upland cropping area in Myanmar, it has suffered from underperformance during the past five decades and been considered as one of the most food-insecure, water-stressed, climate-sensitive, and least-developed regions of the country by the Asia Development Bank (ADB, 2016). Facing the hotter and more erratic rainfall, the conservation agriculture for improved water-use efficiency is imperative in this area (Herridge et al., 2019). In addition to the rice paddy in Central Thailand, the natural deciduous forest and plantation forest in North Cambodia also suffered from the prolonged drought significantly. Consistent with a study based on global EVI (Huang, 2019), higher resistance of tropical evergreen forest than natural deciduous forest and plantation forest was found in EVI and NIR_v (Fig. 9). Previous research has indicated that radiation, rather than water availability, is the main factor to determine tropical evergreen forest productivity (Guan et al., 2015; Saleska et al.,

2016). The increased light exposure under drought could result in enhanced EVI (Huang, 2019). Then, tropical evergreen forest tends to increase canopy light use efficiency in response to drought during the dry season (Tang and Dubayah, 2017), and is less limited by water stress (Guan et al., 2015). Compared to plantation forest, natural deciduous forest would be more vulnerable to drought, evidenced by less changes of \emptyset_F and PAR while comparable suppression of SIF and VI (Fig. 9). At the NF site, the young natural deciduous forest also had a larger decrease of GPP than the mature rubber trees (Fig. 3) under the same drought. It was probably because of the water extraction from the upper soil layers with shorter roots and not fully developed ecosystem among the species (Wang et al., 2022). Additionally, the decreased photosynthesis of plantation forest also related to other types of plantations except for rubber (e.g., coffee, fruit trees, cashews) (Hurni and Fox, 2018).

4.4 Uncertainties in remotely sensed photosynthesis proxies

Although we confirmed usage of SIF in predicting GPP and drought stress effects in TDFs and explored the potential mechanisms behind SIF-GPP_{EC} relationship at the canopy scale, there are still several limitations in our study. We found that SIF had lower correlations to GPP_{EC} than NIR_v and limited performance to capture the maximum GPP_{EC} during the rainy season (Fig. 2). It may be related to the noise and bias in SIF retrieval. As a by-product of photosynthesis, SIF is a small signal (~1% of the absorbed light) and vulnerable to the noise from the strong background of reflected sunlight (Damm et al., 2011). In addition, the large orbital gap of OCO-2 SIF_{native} cannot match flux towers well at the canopy scale, and the expansion of data collecting area may result in an increase of the pixel heterogeneity and scale mismatch. We found a more significant change of SIF_{native} induced by drought, while the variances were larger with the coarser spatial and unfixed temporal resolution (Fig. 8). To over this problem, the contiguous gridded GOSIF and

 $\overline{SIF}_{oco2_005}$ products were produced, but the estimated SIF was still affected by the uncertainties associated with the model training and the input data. $\overline{SIF}_{oco2_005}$ was less sensitive to drought with a larger variance compared to GOSIF and VI at the regional scale. The TROPOspheric Monitoring Instrument (TROPOMI), launched in October 2017 with small footprint size (7 km × 3.5 km) and daily continuous global coverage, could improve SIF significantly (Köhler et al., 2018) and has been used to examine the SIF-GPP relationship (Li and Xiao 2022). TROPOMI SIF was not used in our analysis due to the mismatch of the study periods. Moreover, higher spatial resolution (less than 1 km) is still required to make the footprint truly match the flux tower scale, especially for the highly heterogeneous land cover under human activities. We expect that the upcoming FLEX SIF data with 300-m spatial resolution can better distinguish different vegetation types, and capture vegetation productivity and stress in MSEA.

Moreover, the sun-synchronous satellite cannot provide temporally continuous measurements of SIF due to the fixed local overpass time for a given location, such as 13:30 for the OCO-2. To investigate seasonal SIF-GPP relationships and eliminate the impact of varying incident solar radiation intensities with latitude and time, we converted the remotely sensed instantaneous SIF to the corresponding daily value by applying a daily-mean adjustment factor (Frankenberg et al., 2011) as it has been done in GOSIF and $\overline{SIF}_{oco2_005}$. Previous studies have confirmed the importance of daily adjustment factor in determining the consistency of seasonal SIF-GPP correlation among biomes (Sun et al., 2018; Zhang et al., 2018). However, uncertainty still exists since this correction factor is based on the analytical approximation of solar zenith angle and does not consider the diurnal variation of other environmental factors (e.g., temperature, water stress). A cross-mission comparison of OCO-2 (observed at 13:30) and GOME-2 (observed at 9:30) confirmed the larger reduction of OCO-2 SIF under heat stress in the afternoon than GOME-2 SIF

in the morning by EC measurements and showed higher mean OCO-2 SIF during the growing season (Qiu et al., 2020). The recently launched Orbiting Carbon Observatory-3 (OCO-3) has diurnal sampling capability, and its SIF measurements at different times of day can reveal diurnal cycling of photosynthesis and the mid-day depression in photosynthesis due to water and heat stresses (Xiao et al., 2021). The overlapping tracks of OCO-3 at different times of the day exhibited a larger depression of photosynthesis in the afternoon than in the morning in the dry year by comparing the morning and afternoon retrievals (Zhang et al., 2023). The stomatal limitations and photorespiration are stronger under stresses in the afternoon (Porcar-Castell et al., 2021), while the physiological water stress tends to be diminished in the morning due to the redistribution of soil moisture overnight (Qiu et al., 2020). The specific overpass time of OCO-2 could cause an overestimation of daily averaged photosynthesis and GPP depression under drought. More in-situ SIF measurements at a sub-daily scale are needed to better interpret the GPP-SIF relationship across various ecosystems. The diurnal SIF variation at a large scale will be further elucidated over Americas and Europe by the forthcoming missions such as the NASA Tropospheric Emissions: Monitoring of Pollution (TEMPO) and European Sentinel 4.

606

607

608

609

610

611

612

613

614

615

616

617

618

619

620

621

622

623

624

625

626

627

628

The EC instruments and different carbon partitioning methods for estimating GPP_{EC} would also influence the accuracy of GPP_{EC} (Keenan et al., 2019; Lasslop et al., 2010). We only examined the SIF-GPP relationship at the three TDF sites from two to four years. More sites in the tropical regions, especially with longer data records, are required to further improve our mechanistic understanding of the SIF-GPP relationship. Even though our study found that SIF successfully captured the photosynthesis reduction under drought stress at both the NR and NF sites, the SIF-GPP_{EC} relationship could be decoupled to some extent (Li and Xiao, 2022). Drought stress would reduce carbon assimilation despite of no change in the light reactions of photosynthesis since the

stomatal closure of plants could decrease internal CO₂ concentration and increase photorespiration, often occurring with an increase of heat dissipation in the form of non-photochemical quenching (NPQ), and even caused photoinhibition under severe drought (Helm et al., 2020; Marrs et al., 2020; van der Tol et al., 2014).

5 Conclusions

This study explored the performance of OCO-2 SIF for monitoring ecosystem-scale GPP and the effect of drought on TDFs, which can contribute a better understanding of the mechanisms underlying the SIF-GPP relationships based on the EC measurements. The results reveal that: (1) OCO-2 SIF products had significant linear correlations with daily forest GPP_{EC} at the three sites; (2) NIR_v and SIF products, especially GOSIF, performed well in predicting canopy structure and forest productivity while NDVI and EVI saturated at the two rubber sites due to the high values of LAI; and (3) The SIF-GPP relationships in TDFs were dominantly explained by canopy structure effect, which was represented by NIR_v because it includes both the absorption (fPAR) and scattering (f_{esc}) traits of the canopy structure; (4) \emptyset_F was sensitive to the precipitation anomaly and indicated a large decrease in the eastern MSEA, while its negative effects on SIF was offset by high PAR under drought; (5) Cropland and deciduous forest were more vulnerable to the prolonged drought compared to evergreen forest in MSEA. More observations with higher spatiotemporal resolution and investigations on the effect of physiology in SIF-GPP relationships are highly recommended.

Acknowledgements

The authors would like to acknowledge support from colleagues in Kasetsart University and the French Agricultural Research Center for International Development (CIRAD) for providing flux data at the northern rubber and the southern rubber sites, King Mongkut's University of

| 552 | Technology Thonburi (KMUTT) and International Research Network (IRN) for providing flux |
|-------------------|--|
| 553 | data at the natural forest site. J.X. was supported by the National Science Foundation (NSF) |
| 554 | (Macrosystem Biology & NEON-Enabled Science program: DEB-2017870). We are grateful to |
| 555 | the investigators who made the $\overline{SIF}_{oco2_005}$ product publicly available. We thank the University of |
| 556 | Colorado, Boulder for financing X.W. during this work. |
| 557 | References |
| 558 559 560 | Adachi, M., Ito, A., Ishida, A., Kadir, W.R., Ladpala, P., Yamagata, Y., 2011. Carbon budget of tropical forests in Southeast Asia and the effects of deforestation: An approach using a process-based model and field measurements. Biogeosciences 8, 2635–2647. https://doi.org/10.5194/bg-8-2635-2011 |
| 661 662 663 | Ahrends, A., Hollingsworth, P.M., Ziegler, A.D., Fox, J.M., Chen, H., Su, Y., Xu, J., 2015. Current trends of rubber plantation expansion may threaten biodiversity and livelihoods. Glob. Environ. Chang. 34, 48–58. https://doi.org/10.1016/J.GLOENVCHA.2015.06.002 |
| 664 665 | Badgley, G., Anderegg, L.D.L., Berry, J.A., Field, C.B., 2019. Terrestrial gross primary production: Using NIRV to scale from site to globe. Glob. Chang. Biol. 25, 3731–3740. https://doi.org/10.1111/gcb.14729 |
| 666 667 | Badgley, G., Field, C.B., Berry, J.A., 2017. Canopy near-infrared reflectance and terrestrial photosynthesis. Sci. Adv. 3, 1–6. https://doi.org/10.1126/sciadv.1602244 |
| 668 669 | Baldocchi, D.D., 2020. How eddy covariance flux measurements have contributed to our understanding of Global Change Biology. Glob. Chang. Biol. 26, 242–260. https://doi.org/10.1111/gcb.14807 |
| 570 571 572 | Baldocchi, D.D., 2003. Assessing the eddy covariance technique for evaluating carbon dioxide exchange rates of ecosystems: Past, present and future. Glob. Chang. Biol. 9, 479–492. https://doi.org/10.1046/j.1365-2486.2003.00629.x |
| 573 574 575 | Blackman, C.J., Brodribb, T.J., Jordan, G.J., 2009. Leaf hydraulics and drought stress: response, recovery and survivorship in four woody temperate plant species. Plant. Cell Environ. 32, 1584–1595. https://doi.org/10.1111/J.1365-3040.2009.02023.X |
| 576 577 578 | Burton, C., Rifai, S., Malhi, Y., 2018. Inter-comparison and assessment of gridded climate products over tropical forests during the 2015/2016 El Niño. Philos. Trans. R. Soc. B Biol. Sci. 373, 20170406. https://doi.org/10.1098/rstb.2017.0406 |
| 579 580 | Chabangborn, A., 2014. Asian monsoon over mainland Southeast Asia in the past 25 000 years, Stockholm University. |
| 581 582 | Chaves, M.M., 1991. Effects of Water Deficits on Carbon Assimilation. J. Exp. Bot. 42, 1–16. https://doi.org/10.1093/JXB/42.1.1 |
| 583 584 585 | Chayawat, C., Satakhun, D., Kasemsap, P., Sathornkich, J., Phattaralerphong, J., 2019. Environmental controls on net CO 2 exchange over a young rubber plantation in Northeastern Thailand. ScienceAsia 45, 50–59. https://doi.org/10.2306/scienceasia1513-1874.2019.45.050 |

- Chen, Z., Yu, G., Wang, Q., 2019. Magnitude, pattern and controls of carbon flux and carbon use efficiency in China's typical forests. Glob. Planet. Change 172, 464–473. https://doi.org/10.1016/j.gloplacha.2018.11.004
- Damm, A., Erler, A., Hillen, W., Meroni, M., Schaepman, M.E., Verhoef, W., Rascher, U., 2011. Modeling the impact of spectral sensor configurations on the FLD retrieval accuracy of sun-induced chlorophyll fluorescence. Remote Sens. Environ. 115, 1882–1892. https://doi.org/10.1016/J.RSE.2011.03.011
- Dechant, B., Ryu, Y., Badgley, G., Köhler, P., Rascher, U., Migliavacca, M., Zhang, Y., Tagliabue, G., Guan, K., Rossini, M., Goulas, Y., Zeng, Y., Frankenberg, C., Berry, J.A., 2022. NIRVP: A robust structural proxy for sun-induced chlorophyll fluorescence and photosynthesis across scales. Remote Sens. Environ. 268, 112763. https://doi.org/10.1016/J.RSE.2021.112763
- Dechant, B., Ryu, Y., Badgley, G., Zeng, Y., Berry, J.A., Zhang, Y., Goulas, Y., Li, Z., Zhang, Q., Kang, M., Li, J.,
 Moya, I., 2020. Canopy structure explains the relationship between photosynthesis and sun-induced
 chlorophyll fluorescence in crops. Remote Sens. Environ. 241. https://doi.org/10.1016/j.rse.2020.111733
- Flexas, J., Bota, J., Loreto, F., Cornic, G., biology, T.S.-P., 2004, undefined, 2004. Diffusive and metabolic limitations to photosynthesis under drought and salinity in C3 plants. thieme-connect.com 6, 269–279. https://doi.org/10.1055/s-2004-820867
- Flexas, J., Briantais, J.M., Cerovic, Z., Medrano, H., Moya, I., 2000. Steady-State and Maximum Chlorophyll Fluorescence Responses to Water Stress in Grapevine Leaves: A New Remote Sensing System. Remote Sens. Environ. 73, 283–297. https://doi.org/10.1016/S0034-4257(00)00104-8
- Frankenberg, C., Fisher, J.B., Worden, J., Badgley, G., Saatchi, S.S., Lee, J.E., Toon, G.C., Butz, A., Jung, M.,

 Kuze, A., Yokota, T., 2011. New global observations of the terrestrial carbon cycle from GOSAT: Patterns of plant fluorescence with gross primary productivity. Geophys. Res. Lett. 38, 1–6.

 https://doi.org/10.1029/2011GL048738
- Frankenberg, C., O'Dell, C., Berry, J., Guanter, L., Joiner, J., Köhler, P., Pollock, R., Taylor, T.E., 2014. Prospects for chlorophyll fluorescence remote sensing from the Orbiting Carbon Observatory-2. Remote Sens. Environ. 147, 1–12. https://doi.org/10.1016/j.rse.2014.02.007
- Govindjee, 1995. Sixty-three years since Kautsky: chlorophyll a fluorescence. Aust. J. Plant Physiol. 22: 131–16.
- Grogan, K., Pflugmacher, D., Hostert, P., Mertz, O., Fensholt, R., 2019. Unravelling the link between global rubber price and tropical deforestation in Cambodia. Nat. Plants 5, 47–53. https://doi.org/10.1038/s41477-018-0325-4
- Gu, L., Han, J., Wood, J.D., Chang, C.Y.Y., Sun, Y., 2019. Sun-induced Chl fluorescence and its importance for biophysical modeling of photosynthesis based on light reactions. New Phytol. 223, 1179–1191. https://doi.org/10.1111/nph.15796
- Guan, K., Berry, J.A., Zhang, Y., Joiner, J., Guanter, L., Badgley, G., Lobell, D.B., 2016. Improving the monitoring of crop productivity using spaceborne solar-induced fluorescence. Glob. Chang. Biol. 22, 716–726. https://doi.org/10.1111/gcb.13136
- Guan, K., Pan, M., Li, H., Wolf, A., Wu, J., Medvigy, D., Caylor, K.K., Sheffield, J., Wood, E.F., Malhi, Y., Liang,
 M., Kimball, J.S., Saleska, S.R., Berry, J., Joiner, J., Lyapustin, A.I., 2015. Photosynthetic seasonality of
 global tropical forests constrained by hydroclimate. Nat. Geosci. 8, 284–289.
 https://doi.org/10.1038/ngeo2382
- Hao, D., Asrar, G.R., Zeng, Y., Yang, X., Li, X., Xiao, J., Guan, K., Wen, J., Xiao, Q., Berry, J.A., Chen, M., 2021.
 Potential of hotspot solar-induced chlorophyll fluorescence for better tracking terrestrial photosynthesis. Glob. Chang. Biol. 27, 2144–2158. https://doi.org/10.1111/gcb.15554

- 727 He, B., Liu, J., Guo, L., Wu, X., Xie, X., Zhang, Y., 2018. Recovery of Ecosystem Carbon and Energy Fluxes From the 2003 Drought in Europe and the 2012 Drought in the United States. Geophys. Res. Lett. 4879–4888.
- 728 729 https://doi.org/10.1029/2018GL077518
- 730 He, L., Chen, J.M., Gonsamo, A., Luo, X., Wang, R., Liu, Y., Liu, R., 2018. Changes in the Shadow: The Shifting
- 731 Role of Shaded Leaves in Global Carbon and Water Cycles Under Climate Change. Geophys. Res. Lett. 45,
- 732 5052-5061. https://doi.org/10.1029/2018GL077560
- 733 Helm, L.T., Shi, H., Lerdau, M.T., Yang, X., 2020. Solar-induced chlorophyll fluorescence and short-term 734 photosynthetic response to drought. Ecol. Appl. 30, e02101. https://doi.org/10.1002/eap.2101
- 735 Huang, K., 2019. High ecosystem stability of evergreen broadleaf forests under severe droughts 3494–3503. 736 https://doi.org/10.1111/gcb.14748
- 737 Hurni, K., Fox, J., 2018. The expansion of tree-based boom crops in mainland Southeast Asia: 2001 to 2014. J. Land 738 Use Sci. 13, 198–219. https://doi.org/10.1080/1747423X.2018.1499830
- 739 Ian, H., Osborn, T.J., Phil, J., Lis, D., 2020. Version 4 of the CRU TS monthly high-resolution gridded multivariate 740 climate dataset. Sci. Rep. 1–18. https://doi.org/10.1038/s41597-020-0453-3
- 741 J. Barichivich, T. J. Osborn, I. Harris, G. van der S. and P.D.J., 2021. Monitoring global drought using the self-742 calibrating Palmer Drought Severity. Bull. Am. Meteorol. Soc. 102, S68–S70.
- 743 Joiner, J., Yoshida, Y., Vasilkov, A.P., Schaefer, K., Jung, M., Guanter, L., Zhang, Y., Garrity, S., Middleton, E.M., 744 Huemmrich, K.F., Gu, L., Belelli Marchesini, L., 2014. The seasonal cycle of satellite chlorophyll
- 745 fluorescence observations and its relationship to vegetation phenology and ecosystem atmosphere carbon
- 746 exchange. Remote Sens. Environ. 152, 375–391. https://doi.org/10.1016/j.rse.2014.06.022
- 747 Kaewthongrach, R., Chidthaisong, A., Charuchittipan, D., Vitasse, Y., Sanwangsri, M., Varnakovida, P.,
- 748 Diloksumpun, S., Panuthai, S., Pakoktom, T., Suepa, T., LeClerc, M.Y., 2020. Impacts of a strong El Niño
- 749 event on leaf phenology and carbon dioxide exchange in a secondary dry dipterocarp forest. Agric. For.
- 750 Meteorol. 287, 107945. https://doi.org/10.1016/j.agrformet.2020.107945
- 751 Kaewthongrach, R., Vitasse, Y., Lamjiak, T., Chidthaisong, A., 2019. Impact of Severe Drought during the Strong 752 2015/2016 El Nino on the phenology and survival of secondary dry dipterocarp species in Western Thailand.
- 753 Forests 10, 1–19. https://doi.org/10.3390/f10110967
- 754 Keenan, T.F., Migliavacca, M., Papale, D., Baldocchi, D., Reichstein, M., Torn, M., Wutzler, T., 2019. Widespread 755 inhibition of daytime ecosystem respiration. Nat. Ecol. Evol. 3, 407–415. https://doi.org/10.1038/s41559-019-
- 756 0809-2
- 757 Köhler, P., Frankenberg, C., Magney, T.S., Guanter, L., Joiner, J., Landgraf, J., 2018. Global Retrievals of Solar-
- 758 Induced Chlorophyll Fluorescence With TROPOMI: First Results and Intersensor Comparison to OCO-2.
- 759 Geophys. Res. Lett. 45, 10,456-10,463. https://doi.org/10.1029/2018GL079031
- 760 Kondo, M., Ichii, K., Patra, P.K., Canadell, J.G., Poulter, B., Sitch, S., Calle, L., Liu, Y.Y., Van Dijk, A.I.J.M.,
- 761 Saeki, T., Saigusa, N., Friedlingstein, P., Arneth, A., Harper, A., Jain, A.K., Kato, E., Koven, C., Li, F., Pugh,
- 762 T.A.M., Zaehle, S., Wiltshire, A., Chevallier, F., Maki, T., Nakamura, T., Niwa, Y., Rödenbeck, C., 2018.
- 763 Land use change and El Niño-Southern Oscillation drive decadal carbon balance shifts in Southeast Asia. Nat.
- 764 Commun. 9, 1–11. https://doi.org/10.1038/s41467-018-03374-x
- 765 Lasslop, G., Reichstein, M., Papale, D., Richardson, A., Arneth, A., Barr, A., Stoy, P., Wohlfahrt, G., 2010.
- 766 Separation of net ecosystem exchange into assimilation and respiration using a light response curve approach:
- 767 Critical issues and global evaluation. Glob. Chang. Biol. 16, 187–208. https://doi.org/10.1111/j.1365-
- 768 2486.2009.02041.x

- 769 Li, C.C., 1975. Path analysis a primer. Boxwood Press.
- Li, L., Qiu, B., Guo, W., Zhang, Y., Song, Q., Chen, J., 2022. Phenological and physiological responses of the terrestrial ecosystem to the 2019 drought event in Southwest China: Insights from satellite measurements and the SSiB2 model. Int. J. Appl. Earth Obs. Geoinf. 111, 102832. https://doi.org/10.1016/j.jag.2022.102832
- Li, X., Xiao, J., 2019. A global, 0.05-degree product of solar-induced chlorophyll fluorescence derived from OCO-2, MODIS, and reanalysis data. Remote Sens. 11. https://doi.org/10.3390/rs11050517
- Li, X., Xiao, J., He, B., 2018a. Chlorophyll fluorescence observed by OCO-2 is strongly related to gross primary
 productivity estimated from flux towers in temperate forests. Remote Sens. Environ. 204, 659–671.
 https://doi.org/10.1016/j.rse.2017.09.034
- Li, X., Xiao, J., He, B., Altaf Arain, M., Beringer, J., Desai, A.R., Emmel, C., Hollinger, D.Y., Krasnova, A.,
 Mammarella, I., Noe, S.M., Ortiz, P.S., Rey-Sanchez, A.C., Rocha, A. V., Varlagin, A., 2018b. Solar-induced
 chlorophyll fluorescence is strongly correlated with terrestrial photosynthesis for a wide variety of biomes:
 First global analysis based on OCO-2 and flux tower observations. Glob. Chang. Biol. 24, 3990–4008.
- 782 https://doi.org/10.1111/gcb.14297
- Li, X., Xiao, J., Kimball, J.S., Reichle, R.H., Scott, R.L., Litvak, M.E., Bohrer, G., Frankenberg, C., 2020.
 Synergistic use of SMAP and OCO-2 data in assessing the responses of ecosystem productivity to the 2018
 U.S. drought. Remote Sens. Environ. 251, 112062. https://doi.org/10.1016/j.rse.2020.112062
- Liu, J., Bowman, K.W., Schimel, D.S., Parazoo, N.C., Jiang, Z., Lee, M., Bloom, A.A., Wunch, D., Frankenberg,
 C., Sun, Y., O'Dell, C.W., Gurney, K.R., Menemenlis, D., Gierach, M., Crisp, D., Eldering, A., 2017.
 Contrasting carbon cycle responses of the tropical continents to the 2015–2016 El Niño. Science (80-.). 358.
 https://doi.org/10.1126/science.aam5690
- Ma, H., Cui, T., Cao, L., 2023. Monitoring of Drought Stress in Chinese Forests Based on Satellite Solar-Induced
 Chlorophyll Fluorescence and Multi-Source Remote Sensing Indices. Remote Sens. 15.
 https://doi.org/10.3390/rs15040879
- Manomaiphiboon, K., Octaviani, M., Torsri, K., Towprayoon, S., 2013. Projected changes in means and extremes of temperature and precipitation over Thailand under three future emissions scenarios. Clim. Res. 58, 97–115. https://doi.org/10.3354/cr01188
- Marrs, J.K., Reblin, J.S., Logan, B.A., Allen, D.W., Reinmann, A.B., Bombard, D.M., Tabachnik, D., Hutyra, L.R.,
 2020. Solar-Induced Fluorescence Does Not Track Photosynthetic Carbon Assimilation Following Induced
 Stomatal Closure. Geophys. Res. Lett. 47, e2020GL087956. https://doi.org/10.1029/2020GL087956
- Monteith, J.L., 1977. Climate and the efficiency of crop production in Britain. Philos. Trans. R. Soc. London. B, Biol. Sci. 281, 277–294. https://doi.org/10.1098/rstb.1977.0140
- Monteith, J.L., 1972. Solar Radiation and Productivity in Tropical Ecosystems. J. Appl. Ecol. 9, 747. https://doi.org/10.2307/2401901
- Müller, P., Li, X.P., Niyogi, K.K., 2001. Non-Photochemical Quenching. A Response to Excess Light Energy. Plant Physiol. 125, 1558–1566. https://doi.org/10.1104/PP.125.4.1558
- Olson, D.M., Dinerstein, E., Wikramanayake, E.D., Burgess, N.D., Powell, G.V.N., Underwood, E.C., D'Amico, J.A., Itoua, I., Strand, H.E., Morrison, J.C., Loucks, C.J., Allnutt, T.F., Ricketts, T.H., Kura, Y., Lamoreux, J.F., Wettengel, W.W., Hedao, P., Kassem, K.R., 2001. Terrestrial ecoregions of the world: A new map of life on Earth. Bioscience 51, 933–938. https://doi.org/10.1641/0006-3568(2001)051[0933:TEOTWA]2.0.CO;2
- Palmer, W.C., 1965. Meteorological Drought. US Dep. Commer. Weather Bur. 30, 58.

- 810 Parazoo, N.C., Magney, T., Norton, A., Raczka, B., Bacour, C., Maignan, F., Baker, I., Zhang, Y., Qiu, B., Shi, M.,
- 811 MacBean, N., Bowling, D.R., Burns, S.P., Blanken, P.D., Stutz, J., Grossmann, K., Frankenberg, C., 2020.
- 812 Wide discrepancies in the magnitude and direction of modeled solar-induced chlorophyll fluorescence in
- 813 response to light conditions. Biogeosciences 17, 3733-3755. https://doi.org/10.5194/bg-17-3733-2020
- 814 Porcar-Castell, A., Malenovský, Z., Magney, T., Van Wittenberghe, S., Fernández-Marín, B., Maignan, F., Zhang,
- 815 Y., Maseyk, K., Atherton, J., Albert, L.P., Robson, T.M., Zhao, F., Garcia-Plazaola, J.I., Ensminger, I.,
- 816 Rajewicz, P.A., Grebe, S., Tikkanen, M., Kellner, J.R., Ihalainen, J.A., Rascher, U., Logan, B., 2021.
- 817 Chlorophyll a fluorescence illuminates a path connecting plant molecular biology to Earth-system science.
- 818 Nat. Plants 7, 998–1009. https://doi.org/10.1038/s41477-021-00980-4
- 819 Portillo-Quintero, C., Sanchez-Azofeifa, A., Calvo-Alvarado, J., Quesada, M., do Espirito Santo, M.M., 2015. The
- 820 role of tropical dry forests for biodiversity, carbon and water conservation in the neotropics: lessons learned
- 821 and opportunities for its sustainable management. Reg. Environ. Chang. https://doi.org/10.1007/s10113-014-
- 822 0689-6
- 823 Qian, X., Qiu, B., Zhang, Y., 2019. Widespread decline in vegetation photosynthesis in Southeast Asia due to the
- 824 prolonged drought during the 2015/2016 El Niño. Remote Sens. 11. https://doi.org/10.3390/rs11080973
- 825 Oiu, B., Ge, J., Guo, W., Pitman, A.J., Mu, M., 2020. Responses of Australian Dryland Vegetation to the 2019 Heat
- 826 Wave at a Subdaily Scale. Geophys. Res. Lett. 47, 1-8. https://doi.org/10.1029/2019GL086569
- 827 Qiu, R., Han, G., Ma, X., Xu, H., Shi, T., Zhang, M., 2020. A Comparison of OCO-2 SIF, MODIS GPP, and
- 828 GOSIF Data from Gross Primary Production (GPP) Estimation and Seasonal Cycles in North America.
- 829 Reichstein, M., Bahn, M., Ciais, P., Frank, D., Mahecha, M.D., Seneviratne, S.I., Zscheischler, J., Beer, C.,
- 830 Buchmann, N., Frank, D.C., Papale, D., Rammig, A., Smith, P., Thonicke, K., Van Der Velde, M., Vicca, S.,
- 831 Walz, A., Wattenbach, M., 2013. Climate extremes and the carbon cycle. Nature 500, 287–295.
- 832 https://doi.org/10.1038/nature12350
- 833 Reichstein, M., Falge, E., Baldocchi, D., Papale, D., Aubinet, M., Berbigier, P., Bernhofer, C., Buchmann, N.,
- 834 Gilmanov, T., Granier, A., Grünwald, T., Havránková, K., Ilvesniemi, H., Janous, D., Knohl, A., Laurila, T.,
- 835 Lohila, A., Loustau, D., Matteucci, G., Meyers, T., Miglietta, F., Ourcival, J.M., Pumpanen, J., Rambal, S.,
- 836 Rotenberg, E., Sanz, M., Tenhunen, J., Seufert, G., Vaccari, F., Vesala, T., Yakir, D., Valentini, R., 2005. On
- 837 the separation of net ecosystem exchange into assimilation and ecosystem respiration: Review and improved
- 838 algorithm. Glob. Chang. Biol. 11, 1424–1439. https://doi.org/10.1111/j.1365-2486.2005.001002.x
- 839 Rosseel, Y., 2012. lavaan: an R package for structural equation modeling and more Version 0.5-12 (BETA).
- 840 Saah, D., Tenneson, K., Poortinga, A., Nguyen, Q., Chishtie, F., Aung, K.S., Markert, K.N., Clinton, N., Anderson,
- 841 E.R., Cutter, P., Goldstein, J., Housman, I.W., Bhandari, B., Potapov, P. V., Matin, M., Uddin, K., Pham,
- 842 H.N., Khanal, N., Maharjan, S., Ellenberg, W.L., Bajracharya, B., Bhargava, R., Maus, P., Patterson, M.,
- 843 Flores-Anderson, A.I., Silverman, J., Sovann, C., Do, P.M., Nguyen, G. V., Bounthabandit, S., Aryal, R.R.,
- 844 Myat, S.M., Sato, K., Lindquist, E., Kono, M., Broadhead, J., Towashiraporn, P., Ganz, D., 2020. Primitives
- 845 as building blocks for constructing land cover maps. Int. J. Appl. Earth Obs. Geoinf. 85.
- https://doi.org/10.1016/J.JAG.2019.101979 846

Global 500 m V006.

850

- 847 Saleska, S.R., Wu, J., Guan, K., Araujo, A.C., Huete, A., Nobre, A.D., Restrepo-coupe, N., 2016. Dry-season 848 greening of Amazon forests. Nature 224, 2014–2016. https://doi.org/10.1038/nature16457
- 849 Schaaf, C., Wang, Z., 2015. MCD43A4 MODIS/Terra+ Aqua BRDF/Albedo Nadir BRDF Adjusted RefDaily L3
- 851 Siyum, Z.G., 2020. Tropical dry forest dynamics in the context of climate change: syntheses of drivers, gaps, and 852

- Sjöström, M., Zhao, M., Archibald, S., Arneth, A., Cappelaere, B., Falk, U., de Grandcourt, A., Hanan, N., Kergoat, L., Kutsch, W., Merbold, L., Mougin, E., Nickless, A., Nouvellon, Y., Scholes, R.J., Veenendaal, E.M., Ardö,
- J., 2013. Evaluation of MODIS gross primary productivity for Africa using eddy covariance data. Remote
- 856 Sens. Environ. 131, 275–286. https://doi.org/10.1016/j.rse.2012.12.023
- Song, L., Guanter, L., Guan, K., You, L., Huete, A., Ju, W., Zhang, Y., 2018. Satellite sun-induced chlorophyll fluorescence detects early response of winter wheat to heat stress in the Indian Indo-Gangetic Plains. Glob. Chang. Biol. 24, 4023–4037. https://doi.org/10.1111/GCB.14302
- Song, Q.H., Tan, Z.H., Zhang, Y.P., Sha, L.Q., Deng, X.B., Deng, Y., Zhou, W.J., Zhao, J.F., Zhao, J. Bin, Zhang,
 X., Zhao, W., Yu, G.R., Sun, X.M., Liang, N.S., Yang, L.Y., 2014. Do the rubber plantations in tropical China act as large carbon sinks? IForest 7, 42–47. https://doi.org/10.3832/ifor0891-007
- Sun, Y., Frankenberg, C., Jung, M., Joiner, J., Guanter, L., Köhler, P., Magney, T., 2018. Overview of Solar-Induced chlorophyll Fluorescence (SIF) from the Orbiting Carbon Observatory-2: Retrieval, cross-mission comparison, and global monitoring for GPP. Remote Sens. Environ. 209, 808–823. https://doi.org/10.1016/j.rse.2018.02.016
- Sun, Y., Frankenberg, C., Wood, J.D., Schimel, D.S., Jung, M., Guanter, L., Drewry, D.T., Verma, M., Porcar-Castell, A., Griffis, T.J., Gu, L., Magney, T.S., Köhler, P., Evans, B., Yuen, K., 2017. OCO-2 advances photosynthesis observation from space via solar-induced chlorophyll fluorescence. Science (80-.). 358. https://doi.org/10.1126/science.aam5747
- 871 Sun, Y., Fu, R., Dickinson, R., Joiner, J., Frankenberg, C., Gu, L., Xia, Y., Fernando, N., 2015. Drought onset mechanisms revealed by satellite solar-induced chlorophyll fluorescence: Insights from two contrasting extreme events. J. Geophys. Res. G Biogeosciences 120, 2427–2440. https://doi.org/10.1002/2015JG003150
- Tang, H., Dubayah, R., 2017. Light-driven growth in Amazon evergreen forests explained by seasonal variations of vertical canopy structure. Proc. Natl. Acad. Sci. U. S. A. 114, 2640–2644. https://doi.org/10.1073/PNAS.1616943114/SUPPL_FILE/PNAS.201616943SI.PDF
- Tezara, W., Mitchell, V.J., Driscoll, S.D., Lawlor, D.W., 1999. Water stress inhibits plant photosynthesis by decreasing coupling factor and ATP 401.
- Thorn, A.M., Xiao, J., Ollinger, S. V., 2015. Generalization and evaluation of the process-based forest ecosystem model PnET-CN for other biomes. Ecosphere 6, 1–27. https://doi.org/10.1890/ES14-00542.1
- Tol, C. van der, Berry, J.A., Campbell, P.K.E., Rascher, U., 2014. Models of fluorescence and photosynthesis for interpretingmeasurements of solar-induced chlorophyll fluorescence. J. Geophys. Res. Biogeosciences 119, 2312–2327. https://doi.org/10.1002/2014JG002713.We
- Trenberth, K.E., Dai, A., Van Der Schrier, G., Jones, P.D., Barichivich, J., Briffa, K.R., Sheffield, J., 2014. Global warming and changes in drought. Nat. Clim. Chang. 4, 17–22. https://doi.org/10.1038/nclimate2067
- U.S. DOE, 2012. Research priorities for tropical ecosystems under climate change workshop report.
- Van Der Schrier, G., Barichivich, J., Briffa, K.R., Jones, P.D., 2013. A scPDSI-based global data set of dry and wet spells for 1901–2009. J. Geophys. Res. Atmos. 118, 4025–4048. https://doi.org/10.1002/JGRD.50355
- Verma, M., Schimel, D., Evans, B., Frankenberg, C., Beringer, J., Drewry, D.T., Magney, T., Marang, I., Hutley, L.,
 Moore, C., Eldering, A., 2017. Effect of environmental conditions on the relationship between solar-induced
 fluorescence and gross primary productivity at an OzFlux grassland site. J. Geophys. Res. Biogeosciences
 122, 716–733. https://doi.org/10.1002/2016JG003580

- Wang, C., Beringer, J., Hutley, L.B., Cleverly, J., Li, J., Liu, Q., Sun, Y., 2019. Phenology Dynamics of Dryland Ecosystems Along the North Australian Tropical Transect Revealed by Satellite Solar-Induced Chlorophyll Fluorescence. Geophys. Res. Lett. 46, 5294–5302. https://doi.org/10.1029/2019GL082716
- Wang, S., Zhang, Y., Ju, W., Porcar-castell, A., Ye, S., Zhang, Z., Brümmer, C., Urbaniak, M., Mammarella, I.,

 Juszczak, R., Boersma, K.F., 2020. Warmer spring alleviated the impacts of 2018 European summer heatwave
 and drought on vegetation photosynthesis. Agric. For. Meteorol. 295, 108195.

 https://doi.org/10.1016/j.agrformet.2020.108195
- Wang, X., Blanken, P.D., Kasemsap, P., Petchprayoon, P., Thaler, P., Nouvellon, Y., Gay, F., Chidthaisong, A.,
 Sanwangsri, M., Chayawat, C., Chantuma, P., Sathornkich, J., Kaewthongrach, R., Satakhun, D.,
 Phattaralerphong, J., 2022. Carbon and Water Cycling in Two Rubber Plantations and a Natural Forest in
 Mainland Southeast Asia. J. Geophys. Res. Biogeosciences 127, e2022JG006840.
 https://doi.org/10.1029/2022JG006840
- 905 Wells, N., Goddard, S., Hayes, M.J., 2004. A self-calibrating Palmer Drought Severity Index. J. Clim. 17, 2335– 2351. https://doi.org/10.1175/1520-0442(2004)017<2335:ASPDSI>2.0.CO;2
- Wohlfart, C., Wegmann, M., Leimgruber, P., 2014. Mapping Threatened Dry Deciduous Dipterocarp Forest in
 South-East Asia for Conservation Management. Trop. Conserv. Sci. 7, 597–613.
 https://doi.org/10.1177/194008291400700402
- Wood, J.D., Griffis, T.J., Baker, J.M., Frankenberg, C., Verma, M., Yuen, K., 2017. Multiscale analyses of solar-induced florescence and gross primary production. Geophys. Res. Lett. 44, 533–541.
 https://doi.org/10.1002/2016GL070775
- Wu, X., Xiao, X., Zhang, Y., He, W., Wolf, S., Chen, J., He, M., Gough, C.M., Qin, Y., Zhou, Y., Doughty, R.,
 Blanken, P.D., 2018. Spatiotemporal consistency of four gross primary production products and solar-induced chlorophyll fluorescence in response to climate extremes across CONUS in 2012. J. Geophys. Res.
 Biogeosciences 1–22. https://doi.org/10.1029/2018JG004484
- Xiao, C., Li, P., Feng, Z., Yang, Y., You, Z., Lin, Y., Zhang, X., 2021. Latest 30-m map of mature rubber
 plantations in Mainland Southeast Asia and Yunnan province of China: Spatial patterns and geographical characteristics. Prog. Phys. Geogr. https://doi.org/10.1177/0309133320983746
- Xiao, J., Chevallier, F., Gomez, C., Guanter, L., Hicke, J.A., Huete, A.R., Ichii, K., Ni, W., Pang, Y., Rahman, A.F.,
 Sun, G., Yuan, W., Zhang, L., Zhang, X., 2019. Remote sensing of the terrestrial carbon cycle: A review of advances over 50 years. Remote Sens. Environ. 233, 111383. https://doi.org/10.1016/j.rse.2019.111383
- Xiao, X., Zhang, Q., Braswell, B., Urbanski, S., Boles, S., Wofsy, S., Moore, B., Ojima, D., 2004. Modeling gross
 primary production of temperate deciduous broadleaf forest using satellite images and climate data. Remote
 Sens. Environ. 91, 256–270. https://doi.org/10.1016/J.RSE.2004.03.010
- Xu, H., Xiao, J., Zhang, Z., 2020. Heatwave effects on gross primary production of northern mid-latitude ecosystems. Environ. Res. Lett. 15, 074027. https://doi.org/10.1088/1748-9326/AB8760
- Yang, J., Tian, H., Pan, S., Chen, G., Zhang, B., Dangal, S., 2018. Amazon drought and forest response: Largely reduced forest photosynthesis but slightly increased canopy greenness during the extreme drought of 2015/2016. Glob. Chang. Biol. 24, 1919–1934. https://doi.org/10.1111/GCB.14056
- Yang, L.-Y., Yu, R., Wu, J., Zhang, Y., Kosugi, Y., Restrepo-Coupe, N., Huete, A., Zhang, J., Liu, Y.-H., Zhang,
 X., Liu, W.-J., Zhao, J.-F., Zeng, J., Song, Q.-H., Chen, Y.-J., Song, L., Tan, Z.-H., 2022. Asian tropical
 forests assimilating carbon under dry conditions: water stress or light benefits? J. Plant Ecol.
- 934 https://doi.org/10.1093/JPE/RTAC106

935 Yoshida, Y., Joiner, J., Tucker, C., Berry, J., Lee, J.E., Walker, G., Reichle, R., Koster, R., Lyapustin, A., Wang, Y., 936 2015. The 2010 Russian drought impact on satellite measurements of solar-induced chlorophyll fluorescence: 937 Insights from modeling and comparisons with parameters derived from satellite reflectances. Remote Sens. 938 Environ. 166, 163–177. https://doi.org/10.1016/j.rse.2015.06.008 939 Yu, L., Wen, J., Chang, C.Y., Frankenberg, C., Sun, Y., 2019. High-Resolution Global Contiguous SIF of OCO-2. 940 Geophys. Res. Lett. 46, 1449–1458. https://doi.org/10.1029/2018GL081109 941 Zeng, Y., Badgley, G., Dechant, B., Ryu, Y., Chen, M., Berry, J.A., 2019. A practical approach for estimating the 942 escape ratio of near-infrared solar-induced chlorophyll fluorescence. Remote Sens. Environ. 232, 111209. 943 https://doi.org/10.1016/j.rse.2019.05.028 944 Zhang, T., Zhou, J., Yu, P., Li, J., Kang, Y., Zhang, B., 2023. Response of ecosystem gross primary productivity to 945 drought in northern China based on multi-source remote sensing data. J. Hydrol. 616. 946 https://doi.org/10.1016/J.JHYDROL.2022.128808 947 Zhang, Y., Joiner, J., Alemohammad, S.H., Zhou, S., Gentine, P., 2018. A global spatially Continuous Solar Induced 948 Fluorescence (CSIF) dataset using neural networks. Biogeosciences 15, 5779–5800. 949 https://doi.org/10.5194/bg-2018-255 950 Zhang, Z., Guanter, L., Porcar-Castell, A., Rossini, M., Pacheco-Labrador, J., Zhang, Y., 2023. Global modeling 951 diurnal gross primary production from OCO-3 solar-induced chlorophyll fluorescence. Remote Sens. Environ. 952 285, 113383. https://doi.org/10.1016/J.RSE.2022.113383 953 Zhang, Z., Zhang, Y., Porcar-Castell, A., Joiner, J., Guanter, L., Yang, X., Migliavacca, M., Ju, W., Sun, Z., Chen, 954 S., Martini, D., Zhang, Q., Li, Z., Cleverly, J., Wang, H., Goulas, Y., 2020. Reduction of structural impacts 955 and distinction of photosynthetic pathways in a global estimation of GPP from space-borne solar-induced 956 chlorophyll fluorescence. Remote Sens. Environ. 240, 111722. https://doi.org/10.1016/J.RSE.2020.111722

957